Fractal analysis of vascular networks: Insights from morphogenesis

Sylvie Lorthois, Francis Cassot

www.elsevier.com/locate/yjtbi

Fractal analysis of vascular networks: Insights from morphogenesis

Sylvie Lorthois, Francis Cassot

PII: S0022-5193(09)00526-8
DOI: doi:10.1016/j.jtbi.2009.10.037
Reference: YJTBI5765

To appear in: *Journal of Theoretical Biology*

Received date: 16 March 2009
Revised date: 20 October 2009
Accepted date: 29 October 2009

Cite this article as: Sylvie Lorthois and Francis Cassot, Fractal analysis of vascular networks: Insights from morphogenesis, *Journal of Theoretical Biology*, doi:10.1016/j.jtbi.2009.10.037

Fractal analysis of vascular networks: insights from morphogenesis.

Sylvie Lorthois[1],* and Francis Cassot[2]

[1] Institut de Mécanique des Fluides de Toulouse, UMR CNRS/INPT/UPS 5502, Allée du Professeur Camille Soula, 31400 Toulouse Cedex, France.

[2] INSERM U825 "Imagerie Cérébrale et Handicaps Neurologiques", CHU Purpan, Service de Neurologie, 31059 Toulouse Cedex 3, France.

To whom correspondence should be addressed: lorthois@imft.fr

Keywords : Vascular Morphogenesis ; Microcirculation and flow through tissues ; Brain ; Fractals ; Cancer

Abstract (299 words):
Considering their extremely complicated and hierarchical structure, a long standing question in vascular physio-pathology is how to characterize blood vessels patterns, including which parameters to use. Another question is how to define a pertinent taxonomy, with applications to normal development and to diagnosis and/or staging of diseases.

To address these issues, fractal analysis has been applied by previous investigators to a large variety of healthy or pathologic vascular networks whose fractal dimensions have been sought. A review of the results obtained on healthy vascular networks first shows that no consensus has emerged about whether normal networks must be considered as fractals or not.

Based on a review of previous theoretical work on vascular morphogenesis, we argue that these divergences are the signature of a two-step morphogenesis process, where vascular networks form via progressive penetration of arterial and venous quasi-fractal arborescences into a pre-existing homogeneous capillary mesh. Adopting this perspective, we study the multi-scale behavior of generic patterns (model structures constructed as the superposition of homogeneous meshes and quasi-fractal trees) and of healthy intracortical networks in order to determine the artifactual and true components of their multi-scale behavior. We demonstrate that, at least in the brain, healthy vascular structures are a superposition of two components: at low scale, a mesh-like capillary component which becomes homogeneous and space-filling over a cut-off length of order of its characteristic length; at larger scale, quasi-fractal branched (tree-like) structures. Such complex structures are consistent with all previous studies on the multi-scale behavior of vascular structures at different scales, resolving the apparent contradiction about their fractal nature.

Consequences regarding the way fractal analysis of vascular networks should be conducted to provide meaningful results are presented. Finally, consequences for vascular morphogenesis or hemodynamics are discussed, as well as implications in case of pathological conditions, such as cancer.

1. INTRODUCTION

The main function of the blood vascular system in higher vertebrates is to transport oxygen and nutrients to every cell in the peripheral tissue. For that purpose, the vascular system is comprised of three distinct compartments:

- the arteries, which carry blood away from the heart through a divergent arborescence;
- the capillaries, where oxygen and nutrient delivery from blood to tissues, as well as metabolic waste removal, occur and which have therefore to supply the entire volume of the organism;
- the veins, which carry blood back to the heart through a convergent arborescence.

Functionally, these compartments are organized in series: blood flow proceeds from the upstream arteries to the downstream veins through the capillaries. However, their spatial organization is much more complex. First, arterial and venous trees are hierarchical branching structures covering a wide range of diameter scales, from centimeters at heart level to tens of micrometers at their micro-vascular (arteriolar or veinular) extremities. Second, arterial and venous trees interdigitate, with numerous veins observed paralleling the arteries at various scales. Third, despite their close proximity in space, arterial and venous trees are not directly connected to each other, except in pathological situations. Instead, they are connected by their micro-vascular extremities through the capillary network, the smallest vessels of 4-10 μm diameters. This part of the vascular network, composed of arterioles, veinules and capillaries, is embedded within the organ supplied and is called microcirculation. Fourth, there is a marked variability of vascular patterns among organs. Finally, many pathological conditions, such as atherosclerosis, cancers, arteriovenous malformations, infections, stroke, hypertension, diabetes, obesity and Alzheimer's disease, as well as normal aging, induce changes to vessels' morphology or spatial organization.

Owing to their extremely complicated and hierarchical structure, a long standing question in vascular physio-pathology is how to characterize blood vessel patterns, including which relevant parameters to use for that purpose. A subsequent question is how to define a pertinent taxonomy, with applications to normal growth and development and to diagnosis and/or staging of diseases. A further non-resolved problem is to understand how such complex structures can morphologically evolve and how the design and function cross-talk during development to create the adult vascular architecture.

To address these issues, fractal analysis has been applied to a large variety of healthy or pathologic vascular networks whose fractal dimensions (d_f) have been sought (Gazit et al. 1995, Panico & Sterling 1995, Sandau & Kurz 1997, Kirchner et al. 1996, Wilting et al. 1996, Vico et al. 1998, Parsons-Wingerter et al. 1998, Bergman & Ullberg 1998, Baish & Jain 2000, Herman et al 2001, Arlt 2003, Masters 2004, Gaudio et al. 2005, Cassot et al. 2006, Risser et al. 2007). However, from these previous studies, no consensus has emerged about whether normal vascular networks must be considered as fractals (at least within a limited range of scales, *i.e.* quasi-fractals[1]) or not. One of the most recent studies (Risser et al. 2007), performed on very large three-dimensional (3D) datasets of healthy (primate and rat) intra-cortical networks imaged at high resolution, even suggested that their nature is dependent on scale, vascular structures being fractal at small scale and homogeneous at large scale. These discrepancies shed doubt on the potential of fractal analysis as a quantitative staging/diagnosis

[1] Here, the term *quasi-fractal* denotes an object that shows power-law scaling over a finite range of scales, following Halley et al. (2004).

tool and induce confusion on the spatial organization and relevant scales of healthy vascular structures. In turn, this confusion impairs our understanding of normal angiogenesis, because several scenarios of vascular development are invalidated or, on the contrary, confirmed, depending on the real structure of vascular networks. In addition, the relevant approach for modeling blood flows and oxygen transfers is highly dependent on the underlying vascular architecture.

The aim of the present paper is to clarify both the spatial organization and scales of healthy vascular structures and the potential of fractal analysis in this context by a careful mathematical analysis of the significance of fractal dimension estimation in biological vascular patterns. Our hypothesis is that, aside from methodological problems (see Hamburger et al. 1996, Halley et al. (2004) and Russ (1994)), the lack of consensus on the fractal nature of healthy vascular structures is rooted in their morphogenesis, which proceeds in two successive steps, as described in a series of theoretical papers (Fleury & Schwartz 1999, 2000, Nguyen et al. 2006). Indeed, according to these authors, vascular networks form via progressive penetration of arterial and venous arborescences into a previously formed capillary mesh, by means of a laplacian growth mechanism of hemodynamical origin, suggesting that mature vascular structure should be the union of quasi-fractal trees and of a homogeneous capillary mesh.

Adopting this perspective, the multi-scale behavior of two-dimensional (2D) generic patterns constructed as the union of quasi-fractal trees and homogeneous meshes is studied, demonstrating some unexpected features due to effects of finite spatial scales and effects of structure superposition. The same study is also performed for healthy human intra-cortical networks (Cassot et al. 2006). However, determining artifactual and true components of the multi-scale behavior of such complex (generic and "real-life biological") structures necessitate performing a large number of meticulous tests, leading to a long and somehow tedious inspection of the results obtained by various multi-scale tools. Thus, this technical part (methods and original results) is presented in Appendix A.

This paper is organized as follows. In Section 2, the results obtained by fractal analysis of healthy vascular networks by previous investigators are reviewed. In Section 3, an overview of the morphological development of the vascular system is followed by a review of existing vascular branching morphogenesis theoretical models and their predictions regarding the mature vascular architecture. In Section 4, based on these theoretical predictions, 2D well controlled generic patterns are generated by numerical simulation and the conclusions emerging from the study of their multi-scale behavior (as detailed in Appendix A, Section A1) are summarized. Section 5 is focused on the multi-scale behavior of healthy intra-cortical networks, with additional details available in Appendix A, Section A2. In Section 6, the previous results are discussed and a unifying view of the structure of healthy vascular networks is proposed. Methodological recommendations regarding the way fractal analysis of vascular networks should be conducted in order to provide meaningful results are presented. Finally, consequences regarding vascular morphogenesis or hemodynamics are discussed, as well as implications in case of pathological conditions.

2. FRACTAL ANALYSIS OF HEALTHY VASCULAR NETWORKS: A REVIEW

Strictly speaking, biological specimens cannot be considered as fractals. Indeed, a true random fractal must exhibit statistical scale-invariance over an infinity of length scales.

However, the size of the elementary constituents of a biological system (cells) is not very different, in orders of magnitudes, from the size of a complete organ or organism. Therefore, a biological system can at best be a quasi-fractal, *i.e.* exhibit scale invariance within a limited scale range. In addition, beside these *intrinsic* scales limitations, it is technically very challenging to collect morphometric data on sufficiently large volumes of tissue at high resolution (Cassot et al. 2006, Heinzer et al. 2006, Risser et al. 2007). Therefore, almost every previous study of the scale-invariant properties of healthy vascular networks is either limited to the microvascular end of the vascular network (Gazit et al. 1995, Panico & Sterling 1995, Arlt 2003, Gaudio et al. 2005) or to its arterial and/or venous arborescences (Gazit et al. 1995, Sandau & Kurz 1997, Kirchner et al. 1996, Wilting et al. 1996, Vico et al. 1998, Parsons-Wingerter et al. 1998, Bergman & Ullberg 1998, Herman et al 2001, Masters 2004). In the latter studies, the spatial resolution is not sufficient to resolve the capillary vessels, which is evident while looking at typical images of the vascular networks used for such fractal analysis. For example, in Fig. 1(a) of Gazit et al. (1995), the arterial and venous trees suddenly stop after a few branching orders, without any connections between them; whereas in reality, numerous capillaries, such as those displayed in Fig. 1(b) of the same reference, must be present to establish a connection. Consequently, it is not surprising that the fractal dimensions (evaluated either by the box-counting, the sand-box algorithms, or by spectral approaches, see Appendix A, Section A1) are different in these two categories of studies. For a synthetic summary of the 2D box-counting results, see Table 1.

However, despite the dispersion of the results, some meaningful tendencies can be noted. First, all types of quasi-2D vascular networks have been found to be quasi-fractals when observed at low resolution (i.e. without resolved capillaries), see Table 1, upper part. Second, the fractal dimension is higher at high resolution (see Table 1, lower part). Moreover, in three of the four studies focusing on the microcirculatory network, a homogeneous (non-fractal) behavior (d_f=2) has been obtained (Gazit et al. 1995, Panico and Sterling 1995, Baish and Jain 2001). An identical result has been obtained for the brain microvascular vessels in 3D, which have been shown to become volume filling (d_f=3) above a cut-off equals to 96 µm (Cassot et al. 2006). From this point of view, the fractal dimension of 1.86 obtained by Arlt et al. (2002) in the developing CAM is surprising. However, the cut-offs used for obtaining this result are not available, leaving open the possibility of a methodological bias because any estimate of d_f critically depends on the spatial scales used, especially the lower and upper cut-offs (Berntson and Stoll 1997).

The quasi-fractal nature of 2D vascular networks at low resolution (large scale) is consistent with studies performed on corrosion casts of diverse healthy 3D vascular systems (coronary (Kassab (2000) and references therein), pulmonary (Gan et al 1993, Jiang et al. 1994), hepatic (Hahn et al. 2003)). In these studies, the typical scale range spans from 50 µm to organ size and the fractal dimension is derived from the branching and length-order ratios in a variant of the "Horton-Strahler" ordering scheme (Turcotte et al. 1998), evidencing their quasi-fractal nature. An identical result has also been obtained in the brain arterio-venous network, using the same methodology (Cassot et al. 2006).

From these previous studies, it is thus tempting to conclude that vascular networks are quasi-fractal structures at large scale but are homogeneous at low scale, down to some cut-off length. This view is consistent with the usual description of vascular structures as the union of a "tree-like" distribution network and a "mesh-like" capillary network (West et al. 1999, Kassab 2000, Cassot et al. 2006). However, it is in complete contradiction with the conclusions of a recent study (Risser et al. 2007) performed on very large (tens of cubic

millimeters) 3D datasets of healthy intra-cortical networks imaged by high resolution synchrotron tomography (voxel side: 1.4 μm). In this study, using several multi-scale methods, the authors stated ambition is to "*give a new coherent picture of normal and pathological complex vascular structure*" and to "*resolve the apparent contradiction of previous studies for which normal vascular networks have been found to be either fractal or not*". Their analyses indicate that normal cortical vascular networks have scale-invariant fractal properties on small scale from 1.4 μm up to 40 ~ 65 μm and that, above this threshold, vascular networks can be considered as homogeneous. They further define the length scale for which the transition between fractal to non-fractal occurs as being the Representative Elementary Volume (REV) of the vascular structure, in the usual sense given in the porous media literature[2] (Bear 1972).

These results are all the more disconcerting that the methodology used by the authors is very meticulous. The use of very large datasets for the fractal analysis (performed by the box-counting and by the sand box algorithms) leads to clearcut linear trends with very small error bars in the estimated fractal dimensions and cut-offs. The results are confirmed by a complementary analysis of the power spectrum of the avascular space. Thus, to the best of our knowledge, these authors present the first complete study of the multi-scale behavior of a complete 3D vascular network (including arteries, veins and capillaries) at high resolution over three decades of scales. However, we believe that their interpretation of the data is incorrect. Indeed, relying on a series of theoretical papers about vascular morphogenesis (Fleury & Schwartz 1999, 2000, Nguyen et al. 2006), we will construct simple examples demonstrating that the usual multi-scale tools can lead to counter-intuitive results when the structures under study are not true fractals. For that purpose, the main features of vascular morphogenesis are first introduced.

3. VASCULAR BRANCHING MORPHOGENESIS: PREDICTIONS REGARDING THE MATURE VASCULAR ARCHITECTURE

In this Section, after an overview of the morphological development of the vascular system, models of vascular branching morphogenesis will be reviewed, as well as their predictions regarding the mature vascular architecture.

It is first noteworthy that models of branched growth in biology must provide a reasonable phylogeny (Fleury 2000, Fleury & Schwartz 2001), *i.e.* be compatible with their emergence during the evolutionary history of species, as well as a realistic ontogeny (Murray 1995), *i.e.* be based on the real biological situation and try to isolate the key steps of the growth process. Indeed, although one of the recurrent ideas behind the study of the multi-scale behavior of vascular networks is that it is potentially useful in revealing the physical mechanisms underlying their morphogenesis (Gazit et al. 1995, Bergman & Ullberg 1998, Baish & Jain 2000, Masters 2004, Cassot et al. 2006), several authors warn that two branching patterns with the same fractal dimension have not necessarily been formed by the same class of fundamental processes (Vico et al. 1998, Murray 1995, Meakin et al. 2001, Fleury & Schwartz 2001). In case of vascular morphogenesis, models must thus be consistent with the morphogenetic events and dynamics known to be involved in the formation of new vascular structures.

[2] REV: scale at which the porous medium may be considered as a continuum.

Schematically, the growth of a mature vascular structure begins by the formation of a network of interconnected capillaries, called a capillary plexus, which can develop by two distinct mechanisms, vasculogenesis and angiogenesis (Risau 1997, Patan 2000). The term *vasculogenesis* denotes the process by which randomly distributed precursor cells coalesce to form a network of interconnected capillary tubes. The term *angiogenesis* is the process by which capillary vessels are forming from pre-existing ones, which emit sprouts (sprouting) or are split into two distinct vessels along their axis (intussusception). Vasculogenesis is typically observed in early phases of embryogenesis, where the first capillary plexi form before the onset of plasma or blood perfusion. It is also responsible for the vascularization of organs appearing later, such as the lung and spleen. After onset of perfusion, angiogenesis allows the expansion of previously formed capillary plexi as well as the vascularization of so far avascular regions, such as the brain. Mathematical models of *vasculogenesis* (see Tosin et al. 2006 and references therein), *angiogenesis* (see Mantzaris et al. 2004, Plank & Sleeman 2004, Codling et al. 2008 and references therein) or *both* (Merks et al., 2008) have been proposed but their description is beyond the scope of this paper, which focuses on the later stages.

These newly formed vascular plexi are rapidly remodeled into structures resembling the mature branching pattern. To a large extent, this remodeling is linked to hemodynamics, such that non-perfused capillaries regress whereas vessels undergoing a large flow are likely to enlarge (Risau 1997, le Noble et al. 2004). It begins as soon as blood circulation is established in a given organ (either because the onset of heart beat or because individual capillary sprouts join to form a connected network (Patan 2000)). In chick embryos, when blood circulation fails to establish, *e.g.* after heart removal, capillary plexi fail to remodel, although continuing to grow for several days (le Noble et al. 2004). Furthermore, manipulation of blood flow, for example by ligation of an artery, dramatically affects the final vascular pattern (Nguyen et al. 2006, le Noble et al. 2004).

Thus, the formation of the mature vascular system occurs by progressive selection of small capillaries from a previously formed capillary network, so that every large vessel in the hierarchical branching vasculature was once a vessel of the smallest size (Risau et al. 1997).

To our knowledge, only few models (Honda & Yoshizato 1997, Gödde & Kurz 2001, Fleury & Schwartz 1999, 2000, Nguyen et al. 2006) account for this fundamental feature. However, Honda & Yoshizato (1997) do not reproduce the interdigitation of arterial and venous arborescences, whereas Gödde & Kurz (2001), while producing interdigitating vascular patterns, begin with an initial stochastic capillary growth phase which ends "*as soon as supplying and draining vessel structures approach each other*". In other words, in their model, there is no *intrinsic* mechanism to avoid the direct shunting between arterial sources and venous sinks. Yet, such a mechanism has been recently elucidated: as they grow, arterial vessels progressively disconnect from the surrounding capillaries. This disconnection progressively moves the arterial sources for the blood entering the capillary plexus toward the distal end of the arterial arborescence and avoids direct proximal shunting. This mechanism has been confirmed by experiments on the developing chicken yolk-sac (le Noble et al. 2004) after having been suggested by Fleury and Schwartz (1999) in a simple model of shear-dependent progressive selection of vessels from a previously formed capillary mesh in a laplacian pressure field. For convenience, this simple model has been implemented using classical concepts of statistical physics in which the Laplace equation is approximately solved by performing statistics over the pathways followed by a large number of fictitious random walkers (Courant et al. 1928, Zwillinger 1998). Of course, this methodological trick does not

imply that endothelial cells do walk around until they randomly encounter an existing artery during vascular morphogenesis. For the reader unfamiliar with such statistical methods, a simple illustration is presented in the Appendix B: the Poiseuille flow of a Newtonian fluid in a straight tube, where diffusion is negligible compared to convection and where, as a consequence, fluid particles do not physically behave as random walkers, is solved using fictitious random walkers. The initial approach proposed by Fleury and Schwartz (1999) as well as the progressive improvements introduced in Fleury and Schwartz (2000) and Nguyen et al. (2006) are summarized below, while the justification for using Diffusion Limited Aggregation (DLA) (Witten & Sander 1983) as a tool for progressively selecting the capillaries which become arteries or veins is summarized in Appendix C.

- *Step 1: Initial conditions:* a regular lattice of capillaries must first be provided and the positions of arterial sources and venous sinks, representative of the arterial and venous rudiments allowing the blood circulation to establish in a given organ, must be prescribed. These sources and sinks can have a discrete or a continuous spatial distribution.
- *Step 2: Growth of the arterial tree:* random walkers are iteratively launched from the venous rudiments and grow the arterial tree by DLA. In the DLA original version, a seed particle is fixed at the origin of the coordinate system. Random walkers are iteratively launched at a large distance from the seed and wander randomly over the capillary lattice, until they escape at large distance or they contact the aggregate (*i.e.* the seed at first iteration), to which they stick irreversibly. Here, the seeds for the growing aggregates are the arterial rudiments.
- *Step 3: Arterial disconnection:* the first particles having attached to the arterial aggregate are disconnected from the capillary lattice, such that only a given percentage of the aggregated particles remain active for further growth.
- *Step 4: Growth of the venous tree:* random walkers are launched from the arterial extremities (*i.e.* the active part of the arterial aggregate) to grow the venous tree by DLA. The seeds for the growing venous aggregate are the venous rudiments.
- *Step 5: Effect of tissue growth:* effect of tissue growth has been introduced in Nguyen et al. (2006) but is beyond the scope of this paper.

To our knowledge, this model of vascular morphogenesis is the only model allowing the self-organized generation of realistic vasculatures as well as the prediction of the consequences of localized alterations of blood flow on the arterio-venous global patterning (see Nguyen et al. (2006) where this model is used to generate the entire yolk-sac vasculature, and to predict the effect of an arterial occlusion on its development). It is also the only model allowing a self-consistent description of the connectivity and spatial relationships between arteries, veins and capillaries (Al-Kilani et al. 2007). This model predicts that mature vascular architectures should be quasi-fractal at large scale (DLA trees modified by disconnection and tissue growth), connected by the extremities to a regular lattice of capillaries. Moreover, it predicts that the lower cut-off of the quasi-fractal DLA tree must corresponds to the characteristic length of the capillary lattice. Indeed, in this model, the size of the fictitious random walkers launched to construct the arterial and venous arborescences corresponds to the characteristic size of the capillary mesh, which defines the grid (and pixel) size.

4. FRACTAL ANALYSIS OF GENERIC PATTERNS

In this Section, the multi-scale behavior of generic patterns, constructed as the union of homogeneous meshes and quasi-fractal resampled DLA-type trees (see Fig. 1), is studied. Such a rough model of vascular structure is obviously inspired from the architecture of mature vascular networks predicted by the models of vascular branching morphogenesis described in the previous Section. For control purposes, the multi-scale behavior of their two elementary components (homogeneous mesh and resampled DLA-type tree) is also studied. To this end, the same multi-scale tools as Risser et al. (2007), *i.e.* the box-counting and sand-box algorithms as well as a spectral approach, are used. These methods and the results obtained are presented in Appendix A, Section A1.

The main conclusion of Section A1 is that, when studied using various multi-scale tools implemented following Risser et al. (2007), the two kinds of generic patterns constructed in the present work (Fig. 1) artifactually *appear* to be fractal at low scale and homogeneous at large scale. Indeed, by construction (resampling, see Appendix A, Section A1(a)), a lower cut-off for self-similarity, corresponding to the characteristic length of the capillary lattice, has been imposed to the DLA trees, so that these generic patterns are not fractal at low scale. In addition, these generic patterns are neither homogeneous at large scale due to the presence of the quasi-fractal DLA trees.

Moreover, the results obtained when analyzing the multi-scale behavior of both kinds of generic patterns (Fig. 1) are similar to the results obtained by Risser et al. (2007) when analyzing large datasets of healthy vascular networks imaged at high spatial resolution (see Appendix A, Section A1.(d)). Consequently, based on Risser et al.'s results, it is impossible to conclude that vascular networks are fractal at low scale and homogeneous at large scale. Indeed, the generic patterns introduced in the present work are simple counter-examples: they appear to be, but they are not, fractal at low scale when studied by classic multi-scale tools (box-counting and sand box methods) and by a spectral approach; they are not homogeneous at large scale, due to the presence of the quasi fractals resampled DLA clusters, but they appear to be homogeneous at large scale because of the hindering effect due to the capillary lattice. In addition, the present work demonstrates that Risser et al.'s results can be consistent with the usual description of vascular structures as the union of a "tree-like" distribution network and a "mesh-like" capillary network. As a consequence, they also demonstrate that their results can be consistent with all the previous studies regarding the fractal analysis of healthy vascular structures (see Section 1).

Finally, following the present work, it is tempting to conclude that the cut-off scales, extracted by these authors using the box-counting, the sandbox and the spectral approach, do not correspond to the Representative Elementary Volume (REV) of the vascular structure, but rather give estimates of the characteristic length of the capillary lattice.

To test this hypothesis and to conclude on the nature of vascular networks, it is necessary to study in more detail the capillary lattice of real vascular structures. Indeed, the available data do not permit to decide whether their behavior at low scales (high frequencies) is truly self-similar or artifactual. That is why the following Section is devoted to the fractal analysis of the capillary lattice of healthy intra-cortical networks.

5. FRACTAL ANALYSIS OF INTRA-CORTICAL NETWORKS

In order to progress in the characterization of vascular structures, we have focused on the capillary lattice of healthy human intra-cortical vascular networks (see Fig.2 and Appendix A, Section A2). Using the same multi-scale tools as previously, we have demonstrated that such capillary lattices are space filling over a cut-off length of order 25 to 75 μm, which also gives an estimate of the characteristic length of the capillary lattice. Furthermore, we have shown that the multi-scale tools used are not well-suited to settle on the nature (random or fractal) of the capillary lattice at lower scales, because it is difficult to discriminate between fractality and "*apparent fractality originating from underlying randomness*" (Hamburger et al. 1996, Halley et al. 2004). For example, simple random distributions, such as random distributions of discs at low concentration in 2D, display an apparent fractal behavior between a lower cut-off corresponding to the size of the discs and an upper cut-off which is approximately the average distance between them[3] (Hamburger et al. 1996, Halley et al. 2004).

We have therefore introduced a complementary method, based on the analysis of the regional maxima of the distance map (Fig. 3), to discriminate between both hypotheses. Using this method, the random nature of healthy human intra-cortical capillary lattices has been demonstrated.

In addition, as demonstrated in Section A2.(c), capillary networks become volume-filling over a cut-off of the order of the characteristic size of the capillary mesh. In other words, healthy capillaries fills the available space completely down to this cut-off length and guarantees that no point in the tissue is, on average, further from some point of the vasculature than half of this cut-off. This provides an efficient way for feeding every cell in the interstitial space, the main function of the capillary network.

6. DISCUSSION AND CONCLUSIONS

All together, the present work demonstrates that, at least in the brain, healthy vascular structures are a superposition of two components, which interdigitate: at low scale, a mesh-like capillary component which becomes homogeneous and space-filling over a cut-off length of order of its characteristic length; at larger scale, branched (tree-like) structures which have been systematically demonstrated to be quasi-fractals by others when studied separately from the capillary component (Gazit et al. 1995, Sandau & Kurz 1997, Kirchner et al. 1996, Wilting et al. 1996, Vico et al. 1998, Parsons-Wingerter et al. 1998, Bergman & Ullberg 1998, Herman et al 2001, Masters 2004, Cassot et al. 2006, Kassab 2000, Gan et al. 1993, Jiang et al. 1994, Hahn et al. 2003). Because of the variety of vascular structures considered in these studies (subcutaneous, extra-embryonic, pial, retinal, coronary, pulmonary, hepatic, intra-cortical) and because the homogeneous nature of capillaries has also been demonstrated in various systems (subcutaneous (Gazit et al. 1995, Baish & Jain 2001), epifoveal (Panico &

[3] Indeed, at very low scale (smaller than the diameter of the disks) as well as at very large scales (greater than the typical distance between disks), two space-filling regimes are attained. Between these two regimes, there is a region of reconnection where a linear regime, with a different slope, can be observed, which is entirely an artifact and not caused by self similarity at all (Halley et al 2004). The same phenomenon is observed when studying homogeneous random networks of "thick" capillaries.

Sterling 1995), hepatic (Gaudio et al. 2005)), this conclusion appears to be very general. It immediately implies two additional conclusions:

- First, for the fractal analysis of a given vascular structure to make sense, its two components must be separated beforehand. If not, for scales greater than the characteristic length of the capillary lattice, the tree-like structures are masked. This separation if often *de facto* accomplished by the choice of the observation method. At low resolution, capillaries are automatically removed. At high resolution, due to the necessary compromise between size and resolution, the field of view is usually reduced, thus removing large branched structures. The only exception is when specific techniques are used to image large domains at high resolution (Cassot et al. 2006, Heinzer et al. 2006, Risser et al. 2007). In this case, the capillary lattice must be separated from the tree-like structures, for example by thresholding the vessels hydraulic resistance above a prescribed value (Lauwers et al. 2008). This methodological comment also holds if the vascular structure is intersected with a surface, as for example in histological studies. Indeed, even if in strict mathematical terms, intersecting a fractal object of dimension D with a plane produces a fractal intersection whose dimension is D-1 (Russ 1994), this principle can break down when the structure under study is not an ideal fractal (Halley et al. 2004), leading once again to counter-intuitive results. In addition, this comment must be accounted for if, instead of studying fractal properties, one seeks out the spatial relationships and/or correlations between the large scale (arterial or venous) structures (Al-Kilani et al. 2008).
- Second, taking into consideration these methodological aspects, the description of healthy vascular structures as a superposition of the two components described above is consistent with all the previous studies regarding the multi-scale behavior of vascular structures, briefly reviewed in Section 2. Thus, the present work proposes a unifying view of healthy vascular networks based on arguments related to vascular morphogenesis and should close the controversy regarding the fractal nature of healthy vascular structures.

It should be noted that such a unifying view is compatible with the dual function (distribution and exchange) of the vasculature. Indeed, based on allometric scaling arguments (West et al. 1999), a volume filling structure provides the most efficient way for feeding every cell in the interstitial space, the main function of the capillary network, whereas a fractal distribution network is consistent with the constraint that the time for supplying resources as well as the length of distribution pathways should be minimized. From a transport modeling perspective, this description implies that the complete vascular network can be viewed as the superposition of several coupled flow components:

- a slow homogeneous capillary component, for which the existence of a REV, corresponding to the characteristic capillary length, has been evidenced, and can thus be viewed as a fictitious continuum characterized by effective properties (Bear 1972),
- fast arterial and venous fractal components, which cannot be homogenized because of the absence of any specific length scale, *i.e.* the concept of REV becomes irrelevant. These fractal components can alternately be modeled using a discrete network approach.

Thus, even if it is clear that, from a geometrical perspective, the superposition of these two components remains space-filling at large scale, this complex structure cannot be considered homogeneous at large scale with regard to transport. In the same way, the existence of a homogeneous capillary structure does not imply that the blood flow is homogeneous in the capillaries, in contradiction with experimental measurements in mature micro-vascular beds

(Pries et al. 1990). Indeed, it is well known that significant heterogeneities of the flow parameters (e.g. mean pore velocity) can be observed at *mesoscopic level* (scale of the REV) in homogeneous porous media, resulting from differences in pore size and connectivity. In particular, such heterogeneities can be found in space-filling homogeneous networks, for example in packed bed reactors, i.e. random distributions of spheres or parallel cylinders, even in case of slow flow (Georgiadis et al. 1996): although these structures become homogeneous and space filling above a length scale of the order of the typical distance between spheres or cylinders (Halley 2004, Hamburger 1994), they are still heterogeneous on smaller length scales, exhibiting a large distribution in pore sizes. This also holds for brain microvascular capillary networks, which exhibit a clear heterogeneity in capillary diameters and lengths (Cassot et al. 2006). In addition, in the case of capillary networks, the coupling with the feeding and draining fractal structures (heterogeneous sources and sinks) introduce an additional source of heterogeneity.

The previous description of healthy vascular structures as a superposition of two components is also compatible with the current knowledge of normal vascular morphogenesis, as briefly reviewed in Section 3. Moreover, while the conclusions reached by Risser and al. (2007) are in complete contradiction with the mature vascular structure predicted by the most relevant theory on vascular morphogenesis (Fleury & Schwartz 1999, 2000, Nguyen et al. 2006), the present work constitutes strong support in favor of this theory. Indeed, as observed by Murray (1995) who warns about the abuse of multi-scale analysis in neuroscience, it is essential to "*return to the biology with predictions, comments and suggestions for illuminating experiments*" in order for a theory in this field to be validated. Here, the pitfalls of multi-scale analysis applied to complex experimental data have been understood based on a simple theoretical prediction.

However, it should also be noted that, at present, this conclusion cannot be generalized to pathological conditions. In particular, regarding cancer, the situation is probably more complex. Briefly, when studied at low resolution, tumor vasculatures (obtained by inoculation of various cancerous cell lines in mice bearing dorsal skinfold chambers) have been shown to be fractals, with fractal dimensions ranging approximately from 1.8 to 1.95 (Gazit et al. 1995, Baish & Jain 2000), significantly higher than that of healthy vasculatures. When studied at high resolution over large domains, tumor vasculatures obtained by injection of gliosarcoma cells in rat brains exhibited a complex behavior qualitatively similar to, but quantitatively significantly different from, the behavior of healthy vasculatures (Risser et al. 2007)[4]. From these results, in the same way as for healthy structures, Risser et al. conclude that tumor vasculatures are fractal at low scale but homogeneous at large scale. However, in the same way as for healthy structures, this conclusion is in contradiction with the previous studies of tumor vasculature performed at low resolution (Gazit et al. 1995, Baish & Jain 2000), which, as discussed above, uniquely focus on the large scale structures. Thus, tumor vasculatures are probably the superposition of several components, including fractal components at large scale. However, at low scale, a random homogeneous component must be ruled out, due to the great heterogeneity characteristic of tumors. In order to improve our understanding of their vascular architecture, further work performed over restricted regions imaged at high resolution should

[4] Indeed, the box-counting and sand-box results exhibited two linear domains separated by a clear cut-off. In all cases, above the cut-off, the slope was equal to 3. Below the cut-off, the slope was between 1.9 and 2.4, significantly higher than the slope at low scale obtained for healthy vasculatures. In addition, the cut-off length between these domains was significantly greater for tumors. The power spectrum also exhibited two domains, with a linear decrease at high frequencies and saturation at low frequencies. The cut-off length between these two domains was also significantly greater for tumors.

be conduced. In addition, because the classification of blood vessels (between capillary and non capillary vessels) developed for normal tissues based on structure (anatomy) and function (physiology) may not be applicable to tumors (Gazit et al. 1995, Jain 1988), the relevant criteria for defining and separating these tumor vascular components are still to be found. For example, in tumors such as clear cell renal cell carcinoma, both differentiated and undifferentiated vessels (*i.e.* vessels made up of cells that have grown to the normal mature stage of development and vessels made up of cells that remain in an immature or "primitive" stage) coexist, which could serve as a basis for an alternative classification (Yao et al. 2007). Therefore, it seems to us that the studies aiming at determining a fractal dimension from 2D thin tissue sections of tumor tissues (for example Sabo et al. (2001), Weyn et al. (2004)) must be interpreted with great caution until these methodological issues are resolved. In particular, it is not surprising that the clinical significance of the "fractal dimension" deduced from these studies, as a prognostic indicator of patient survival, is still highly controversial (Sabo et al. 2001, Weyn et al. 2004, Grizzi et al. 2001, Sabo et Resnick 2001).

In summary, the present work meticulously addresses the issues of spatial organization and scales in "real-world" biological structures, highlighting effects of finite spatial scales and effects of structure superposition. It could be of interest in a large number of biological branched structures, from lung to neurons, or non branched structures, such as bone, for which fractal analysis is an increasingly popular staging and/or diagnosis tool.

APPENDICES

APPENDIX A : Technical analysis of complex generic patterns and "real-life" biological structures.

This appendix is devoted to the technical analysis of complex generic patterns (Section A1) and "real-life" biological structures (Section A2). In Section A1, the method for constructing bi-dimensional generic patterns as the union of homogeneous meshes and quasi-fractal DLA trees –imposing a lower cut-off corresponding to the characteristic length of the homogeneous meshes– will first be presented. Then, the multi-scale tools used, as well as the procedures used for their validation, will be described. Finally, the results obtained will be presented and compared to the results obtained by Risser et al. (2007) on very large datasets of healthy intra-cortical networks imaged at high resolution. In Section A2, the datasets used for the analysis of the capillary lattice of human healthy intra-cortical networks will first be presented. Then, the implementation in three-dimensions of the multi-scale tools presented in Section A1 will be described and validated. The results obtained will be subsequently presented. A new multi-scale tool, based on the computation of the regional maxima of the distance map, will then be introduced in order to conclude on the nature of the capillary lattice.

A1. FRACTAL ANALYSIS OF GENERIC PATTERNS

(a) Construction of generic patterns

As argued in Section 3, in a rough approximation, mature vascular structures should be the union of homogeneous capillary meshes and DLA-type trees with a lower cut-off corresponding to the characteristic capillary length. In the whole following, binary structures constructed over 4096 x 4096 domains have been considered. The characteristic length of the capillary lattice, denoted by n, has been fixed to 16.

Two kinds of homogeneous meshes have been considered: n x n square grids and random networks exhibiting a Gaussian distribution of cells' areas. Such networks have been constructed by randomly choosing one point in every elements of a n x n square grid and by subsequently extracting the voronoi diagram of this random set of points (see Fig. A1(A)). In this way, a regular random network has been obtained, with a Gaussian probability distribution function of cell's areas approximately centered on n^2 (see Fig. A1(B) and legend). Indeed, for five realizations, the Gaussian's mean μ was found, by least squares regression, to be 252 ± 0.11 (mean ± sd) and its variance σ^2 was found to be 4126 ± 24, with a coefficient of determination R^2 systematically greater than 0.996.

DLA trees have been generated using dla-nd, an off lattice DLA simulator freely available under the Gnu General Public License at http://markjstock.org/dla-nd/. First, in order to test the multi-scale tools described below, DLA clusters consisting of 500 000 particles have been generated (Fig. A2). However, for such DLA trees, the lower cut-off is equal to one pixel, corresponding to the size of the randomly moving particles. Thus, in order to generate quasi-fractals with a lower cut off equal to n, DLA clusters of 5000 particles have been generated over smaller domains (256 x 256) and subsequently resampled to a final size of 4096 x 4096 by dividing each pixel in n x n pixels areas[5].

[5] This procedure is equivalent to the construction of 5000 particles' DLA clusters over 4096 x 4096 domains using random walkers of size n x n.

Generic patterns have been defined as the union of these quasi-fractals and of either kind of homogeneous meshes (see Fig. 1). By construction, as a lower cut-off for self-similarity has been imposed to the DLA trees, these generic patterns are not fractal at low scale. They are neither homogeneous at large scale due to the presence of the quasi-fractal DLA trees.

(b) Multi-scale tools

The multi-scale tools used in the present work have been chosen following Risser et al. (2007) and have been implemented following the additional details available in Risser (2007). In particular, neither skeletonization nor edge detection was performed prior to analysis. The fractal dimension has been evaluated by box-counting and sand-box methods. As a complement to these approaches, the distance map of the avascular space has been analyzed by a spectral approach.

i. Box-counting and sand-box approaches

Briefly, in the box-counting method, a regular grid of square elements of size r is superimposed to the pattern, and the number $N(r)$ of square elements intersecting the pattern is counted. For a fractal object, the plot of N as a function of r in a bi-logarithmic scale is linear, its slope being opposite to the fractal dimension. Baish et Jain (2001) caution that $N(r)$ depends on the origin chosen for the grid and that the strict estimation of the fractal dimension requires shifting the grid to all possible locations until the minimum value of $N(r)$ is found. However, following Risser (2007), this step was omitted. Nevertheless, in order to avoid coincidences of the box-counting grid with the n x n square grid underlying the resampled DLA, the box-counting origin was shifted by one pixel in both directions of space.

In the sand-box method, a pixel belonging to the pattern is randomly chosen as a centering site. Square boxes of size r (comprised between 3 and 2511) are centered on it and, for boxes totally contained in the 4096 x 4096 domain, the total number of white pixels $N(r)$ falling in each box is counted. The procedure is repeated for a large number η of centering sites. For a fractal object, the plot of the average of N as a function of r in a bi-logarithmic scale is linear, its slope corresponding to the fractal dimension.

Both methods have been validated using originally sampled 500 000 particles DLA clusters (see Fig. A3). The slopes of the bi-logarithmic plots have been sought using the procedure introduced by Berntson and Stoll (1997) for quantitatively determining the spatial scales over which the structure under study shows self-similarity. Briefly, this technique consists in removing extreme points of the plot until a statistical test for curvilinearity becomes negative, *i.e.* the addition of a second order term for fitting the residual plot (*i.e.* plot of the residuals versus values predicted by a linear fit) becomes not significant at the 1% level (Sokal & Rohlf 1994). By this way, the fractal dimension measured using the box-counting method over three realizations was 1.665 ± 0.016. The linear range spanned from 11± 6 to 2048 ± 0 pixels, *i.e.* more than two decades of scales. The fractal dimension measured using the sand-box method was 1.688 ± 0.011. The linear range spanned from 56 ± 21 to 584 ± 382 pixels, *i.e.* one decade. In both cases, the coefficient of determination R^2 was greater than 0.999. These results are in accordance with the theoretical mean-field prediction for DLA in 2D ($d_f=(2^2+1)/(2+1)=1.667$) (Vicsek 1992).

ii. Spectral approach

Classically, in the spectral approach, the fractal dimension is deduced from the Fourier power spectrum of the 2D pattern. For a fractal object, the plot of this power spectrum as a function of the spatial frequency in a bi-logarithmic scale is linear. According to Halley et al. (2004), its fractal dimension is related to the slope s of the plot by $d_f = (5+s)/2$. An alternative version of this classical approach, focusing on the distance map of the avascular space and not on the vascular pattern, has been introduced by Risser et al. (2007). Indeed, the distance map, which represents the distance of any black pixel (tissue point) from the nearest white pixel (vessel) can provide information on the spatial delivery of oxygen by the vascular network. However, it is noteworthy that, from this alternative approach, the fractal dimension of the initial 2D pattern cannot be deduced, because no simple relationship can be drawn between f_d and the slope of the power spectrum of the avascular space's distance map.

Briefly, the distance map $d(i,j)$ of the avascular space is first computed. The Fourier transform of the distance map $\widetilde{d}(f_i, f_j)$ is computed using a bidimensional fast-Fourier transform algorithm, the relevant range of spatial frequencies f_i and f_j lying between the inverse image size 1/(4096 pixels) and the high frequency limit 1/(2 pixels). The power spectrum $P(f_i,f_j)$ is obtained as $|\widetilde{d}(f_i, f_j)|^2$. This power spectrum is finally averaged over concentric circles in the Fourier plane ($f_{ij} = \sqrt{f_i^2 + f_j^2} = cste$) to obtain the averaged power spectrum $P(f_{ij})$. For a fractal avascular space, the plot of P as a function of f_{ij} in bi-logarithmic coordinates is linear.

The spectral approach has first been validated in its classical version by studying the Fourier spectra of originally sampled 500 000 particles DLA clusters. Indeed, these clusters have been demonstrated to be fractal objects by the box-counting and sand-box methods. The slopes of the bi-logarithmic plots have been sought using the same procedure as above. By this way, the linear range over three realizations spanned from 8.6 ± 0 pixel^{-1} to 225.4 ± 42.5 pixel^{-1}, *i.e.* more than one decade of frequency scales. The slope s was -1.55 ± 0.016 with coefficients of determination R^2 greater than 0.995. Thus, the fractal dimension of the 500 000 particles DLA clusters obtained by this method ($d_f = (5+s)/2$) was 1.722 ± 0.008, which slightly overestimates the theoretical prediction (1.667, see above). Second, the alternative approach focusing on the distance maps of the same clusters has been tested. The spectra obtained by this alternative approach were linear ($s = -3.07 \pm 0.008$) with coefficients of determination R^2 greater than 0.999. However, the linear range of frequency scales (51.8 ± 5.7 pixel^{-1} to 163.5 ± 26.5 pixel^{-1}) was reduced compared to the linear range obtained with the classical approach, which is not surprising due to the finite size of the domain under study (side effects).

(c) Multi-scale analysis

In this Section, the box-counting and sand-box methods are successively applied to the 5000 particles resampled DLA clusters, to both kinds of homogeneous meshes and to both kinds of generic patterns (Fig. 1). Then, the distance map of their avascular space is analyzed by the spectral approach.

i. Box-counting and sand-box analyses

First, 5000 particles resampled DLA clusters have been analyzed (see Fig. A4) and the spatial scales over which they show self-similarity have been determined using Berntson's procedure (see Section A1.(b).*i*). By this way, the fractal dimension measured using the box-counting method over five realizations was 1.623 ± 0.003. The linear range spanned from 1 ± 0 to 4096 ± 0 pixels, *i.e.* the whole range of scales for these structures. The fractal dimension measured using the sand-box method was 1.637 ± 0.011. The linear range spanned from 3 ± 0 to 2511 ± 0 pixels, *i.e.* almost three decades. In both cases, the coefficient of determination R^2 was greater than 0.998. Thus, even if a lower cut-off for self-similarity has been imposed while generating these resampled DLAs, *they appear to be self-similar over the whole range of scales when studied by both multi-scale tools*.

Second, the n x n square grid, which is by construction homogeneous for scales above n and a linear object for lower scales, has been analyzed. As expected, in both cases, the plot of N as a function of r in a bi-logarithmic scale exhibits two domains (see Fig. A5). The cut-off length between these two domains has been detected automatically by comparing the local slope $s(r)$ to the slope $\widetilde{S}$ between the data obtained at minimal and maximal box sizes ($\widetilde{S} = (N(r_{max})-N(r_{min}))/(r_{max}-r_{min})$) : for increasing r, the cut-off length r_{cut} is reached as soon as $|s(r)|$ becomes greater than $\left|\widetilde{S}\right|$. By this method, r_{cut} was determined as 12 pixels by the box-counting method and as 39 pixels by the sand-box method, that is to say, lower and upper bound values for n. At larger scale, a homogeneous space-filling behavior (slope $= \pm 2$) is observed. In this domain, linearity of the data was confirmed by use of Berntson's procedure : the linear range spanned from 16 to 4096 pixels (box-counting) and from 51 to 2511 pixels (sand-box), with a coefficient of determination R^2 greater than 0.999. At lower scale, Berntson's statistical test for curvilinearity was always positive at the 1% level. Thus, the linear behavior is only apparent, even if the best linear fit for box sizes smaller than r_{cut} (dotted lines on Fig. A5) has high coefficients of determinations[6]. Thus, both multi-scale tools are able to discriminate between the low scale region, where the square grid is only apparently fractal, and the large scale region, where it is homogeneous and space filling.

The same behavior is observed for random networks (see Fig. A6). For five realizations, r_{cut} was determined as 10 ± 0 pixels (box-counting) and as 25 ± 0 pixels (sand-box), *i.e.* lower and upper bound values for n. At large scale, the linear range spanned from 12 ± 0 pixels to 4096 ± 0 pixels (box-counting) and from 31 ± 0 pixels to 2511 ± 0 pixels (sand-box), with slopes of $-1.999 \pm 4\text{x}10^{-5}$ (box-counting) and $1.999 \pm 3.2\text{x}10^{-4}$ (sand-box) and coefficients of determination greater than 0.999. At low scale, linearity was only apparent, as determined by Berntson's procedure. Thus, as expected, random networks are not fractal at low scale. In addition, both multi-scale tools demonstrate that these networks are homogeneous at large scale.

Third, both kinds of generic patterns (see Fig. 1) have been analyzed. In both cases, the plots of N as a function of r in a bi-logarithmic scale exhibit two linear domains (see Figs. A7 and A8). The cut-off lengths r_{cut} between these domains have been detected automatically as above. The linear ranges of each domain, as well as their slopes, have been determined using Berntson's procedure. The data obtained for five realizations are summarized in Table A1.

[6] Incidentally, this result demonstrates that there is no inconsistency between the results obtained by Arlt et al. (2003) in the developing CAM and the description of capillary networks as homogeneous meshes.

By construction, the union of 5000 particles resampled DLA clusters and of either kind of meshes is not self similar for scales below than n. However, *they appear to be self-similar at low scale when studied by both multi-scale tools*, with fractal dimensions ranging from 1.22 to 1.76 (see Table A1, left). In addition, the self-similar nature of the resampled DLA cluster at large scale is masked by the presence of the superimposed mesh, leading to slopes approximately equal to 2 (Table A1, right). As a conclusion, these multi-scale tools give an estimate of the characteristic length of the underlying (capillary) lattice, because the cut-off values obtained by the box counting and the sand-box methods are respectively a lower bound and an upper bound value for n[7]. However, they are not adapted to study the fractal behavior of the large structures (DLA clusters) when the image resolution is sufficiently high to display the capillary mesh. In addition, they are not adapted to study the lower scales, where they erroneously detect self-similarity.

Therefore, when studying real vascular structures, it is impossible to conclude that they are fractal at low scale and homogeneous at large scale only on the basis of similar results obtained by box-counting and sand-box analyses. That is why it is important to check whether the spectral approach is more robust. For that purpose, in the next sub-section, the spectral approach is applied to the resampled DLA clusters superimposed, or not, to both kinds of homogeneous meshes.

ii. Spectral approach

The averaged power spectra of five realizations of the distance maps of 5000 particles resampled DLA clusters superimposed, or not, to the square grid are displayed on Fig. A9(A). For comparison, the power spectrum of the square grid distance map is displayed on the same figure. First, this spectrum displays clear peaks, the first one at k_c = 256 pixel^{-1}, indicating a periodic structure with a characteristic length l_c of 4096/k_c, *i.e.* 16 pixels, the imposed period of the grid. A plateau at lower frequencies indicates the absence of any specific relevant scale, *i.e.* a homogeneous structure, beyond 16 pixels. Second, the spectrum of the distance maps of the 5000 particles resampled DLA clusters is approximately linear (slope = -3.12 ± 0.13), with a coefficient of determination greater than 0.999, but the linear range according to Berntson's procedure is limited to k_{ij} ranging from 48.5 ± 30.4 pixel^{-1} to 201.5 ± 130 pixel^{-1}. Finally, the spectrum of the distance maps of the superposed structures is linear (slope = -3.99 ± 0.016) for frequencies beyond k_c, with a linear range spanning from k_{ij} = 258.5 ± 0 pixel^{-1} to 2048 ± 0 pixel^{-1}, *i.e.* the whole range of frequencies above k_c, but a coefficient of determination of only 0.76 due to the presence of the frequency peaks. In addition, this spectrum saturates at low frequencies. Thus, as previously, the superposed structures appear to be self-similar at large frequencies (low scale) and homogeneous at low frequencies (large scales) when studied by the spectral approach.

The averaged power spectra of five realizations of 5000 particles resampled DLA clusters superimposed, or not, to random meshes are displayed on Fig. A9(B). For comparison, the averaged power spectrum of the random meshes is displayed on the same figure. A smooth maximum, centered on k_c = 256 pixel^{-1}, is observed in the spectrum of regular meshes, indicating a quasi periodic structure with a characteristic length l_c of 16

[7] Note that the cut-off value obtained by the BC method is directly related to the characteristic length of the capillary mesh whereas the cut-off obtained by the SB method depends on this characteristic length as well as on the relative number of pixels belonging to the DLA cluster and to the capillary lattice (*i.e.* the relative weight of the DLA), in a complex fashion. Therefore, in practice, the BC cut-off provides a better estimate of the characteristic length of the capillary mesh.

pixels. In addition, a plateau at low frequencies (typically below 140 pixel^{-1}) indicates the absence of any specific relevant scales beyond 29 pixels. At large frequencies, however, a linear behavior is observed. According to Bernton's procedure, its linear range spans from k_{ij} = 586.5 ± 5.5 pixel^{-1} to 1258.5 ± 15.8 pixel^{-1} with a slope of -3.9791 ± 0.009 and a coefficient of determination greater than 0.999. The same behavior (slope of -4.000 ± 0.003 with a linear range spanning from k_{ij} = 601.5 ± 4.5 pixel^{-1} to 1262.5 ± 5.5 pixel^{-1}) is observed at high frequencies when resampled DLA clusters are superimposed to the random meshes. In this latter case, saturation of the power spectrum at low frequencies is still observed, even if it is less pronounced than the saturation observed for the meshes alone. Thus, once again, the superposed structures appear to be self-similar at large frequencies (low scale) and homogeneous at low frequencies (large scales) when studied by the spectral approach.

As a conclusion, in the same way as for the box-counting and sand-box methods, the spectral approach is not adapted to study the multi-scale behavior of generic patterns constructed as the union of quasi-fractal trees and homogeneous meshes, because the results obtained are counter-intuitive. In order to seek whether such an idealized generic structure could properly describe a real vasculature such as the intra-cortical vascular network, the results presented above are compared to the results obtained by Risser et al. (2007).

(d) Comparison with the results of Risser et al.

The results obtained when analyzing the multi-scale behavior of both kinds of generic patterns (Fig. 1) are very close to the results obtained by Risser et al. (2007) when analyzing large datasets of healthy vascular networks imaged at high spatial resolution.

First, in the present work, two domains are evidenced by the box-counting and sand box analyses: a linear domain at low scale (note that even if the linear ranges indicated in Table A1, as determined by Berntson's procedure, seems to bee small, the best linear fits for box sizes smaller than the cut-off length, displayed as dotted lines in Figs. A7 and A8, always have coefficients of determinations greater than 0.997). The apparent fractal dimension obtained by the box-counting method for this linear domain is always smaller than the apparent dimension obtained by the sand-box method. In addition, the cut-off lengths between the two domains determined by the box-counting method are always smaller than the cut-off determined by the sand-box method. At higher scale, a homogeneous, space-filling behavior (d_f = 2) is obtained. All these results have also been obtained by Risser et al. (2007), although in 3D, where the homogeneous, space-filling behavior is characterized by d_f = 3.

The most significant difference with their results concerns the spectral approach. Indeed, neither the square grid nor the random networks used in the present work are able to reproduce a clear linear trend at high frequencies (*i.e.* a linear trend over the whole range of frequencies above k_c associated to a large coefficient of determination). In the case of the square grid, the coefficient of determination is low due to the signature of the frequency peaks. In the case of the random networks, the smooth maximum centered on k_c induces a deviation from linearity for frequencies just above k_c, which reduces the range of the linear trend. However, this last effect, due to the quasi-periodic nature of the random meshes constructed in 2D, disappears in 3D (see Fig. A10 and legend). Furthermore, the slope obtained in the 3D case (-4.56) is very close to the slope obtained by Risser et al. (2007) for healthy networks (-4.8 or -4.9).

Consequently, based on Risser et al.'s results, it is impossible to conclude that vascular networks are fractal at low scale and homogeneous at large scale. Indeed, the generic patterns described above are simple counter-examples: they appear to be, but they are not, fractal at low scale when studied by classic multi-scale tools (box-counting and sand box methods) and by a spectral approach; they are not homogeneous at large scale, due to the presence of the quasi fractals resampled DLA clusters, but they appear to be homogeneous at large scale because of the hindering effect due to the capillary lattice.

A2. FRACTAL ANALYSIS OF INTRA-CORTICAL NETWORKS

In this Section, the multi-scale tools described above, but implemented in 3D, are used to analyze intra-cortical capillary networks. Finally, a complementary analysis, based on the analysis of the regional maxima of the distance map of their avascular space, is introduced to conclude on their behavior at low scale.

(a) Datasets

The datasets used for analysis have been previously obtained by Cassot et al. (2006) from thick sections (300 µm) of an india ink-injected human brain (Duvernoy collection, Duvernoy et al. 1981) by confocal laser microscopy, with a spatial resolution of 1.22 µm x 1.22 µm x 3 µm. To study in more details the capillary lattice, six limited areas (256 x 256 x 64 voxels) have been manually selected by visual inspection in the lateral or top region of the collateral sulcus of the temporal lobe: three lateral regions (L1 to L3) and two top regions (S1 and S2), only containing capillaries (*i.e.*, following Cassot et al. (2006), vessels of diameter smaller than 9 µm), as well as one lateral region with capillaries surrounding the distal extremity of an arterial arborescence (LA1). Four of these regions are represented on Fig. 2.

(b) Multi-scale tools in 3D

The box-counting and sand-box methods have first been implemented in 3D as a direct extension of the 2D procedures described in Section A1.(b). Here, as the voxels are not isotropic, the dimensional value of the box side r^* is related to its adimensional value r (in voxels) by a conversion factor equals to the cubic root of the voxel volume. In addition, a pseudo 3D implementation of the sand-box method has been introduced, where parallelepiped boxes of size r x r x 33 are used instead of cubic boxes. In this case, the dimensional value of the box side r^* is simply 1.22 r. With the two former methods, a homogeneous space-filling structure exhibits a fractal dimension of three, whereas with the third method, such a structure exhibits a dimension of two.

In the 3D spectral approach, the distance map of the avascular space $d(i,j,k)$ is first computed in 3D. The Fourier transform of the distance map $\tilde{d}(k_i, k_j, k_k)$ is then computed using a bidimensional fast-Fourier transform algorithm twice in succession. The power spectrum $P(k_i,k_j,k_k)$ is obtained as $|\tilde{d}(k_i, k_j, k_k)|^2$. This power spectrum is first averaged for each k_k over concentric circles in the Fourier plane ($k_{ij} = \sqrt{k_i^2 + k_j^2} = cste$) and finally averaged over k_k to obtain the averaged power spectrum $P(k_{ij})$.

(c) Multi-scale analysis

The results obtained for region L1 by the multi-scale tools described above are displayed on Fig. A11. As previously, the existence of two domains is revealed by the box-counting, the sand-box and the pseudo 3D sand-box methods and the cut-off lengths between these two domains (respectively 26.35, 51.05 and 47.58 μm) have been detected automatically (see Section A1.(c).*i*). Once again, the sand-box cut-offs are greater than the box-counting cut-off. Above these cut-offs, a homogeneous, space-filling behavior is detected by the box-counting and the pseudo 3D sand-box methods (fractal dimension of 3 and 1.949, respectively), whereas the maximal box size attainable by the sand-box method (64 x 64 x 64 voxels, due to the limited depth of the datasets) precludes reaching such a domain, with a slope equal to 2.765. Below these cut-offs, the best linear fit exhibits slopes of -2.179 by box-counting (very close to value of 2.17, interpreted as a fractal dimension, given by Cassot et al. (2006) for the capillaries of a middle layer cortex region) and of 2.06 by sand-box. However, by box-counting, the linearity is only apparent, because Berntson's statistical test for curvilinearity is always positive at the 1% level. Conversely, by sand-box, a linear range at intermediate scales (11.5 to 41.2 μm) with a slope of 1.686 is detected by Berntson's procedure. Below this range, a slope approaching 3 is obtained, due to the 3D nature (at low scale) of the vascular segments studied. However, the linear-range at intermediate scale is not detected when the vascular network contained in region L1 is first skeletonized, suggesting "*apparent fractality originating from underlying randomness*" (Hamburger et al. 1996, Halley et al. 2004)[8]. Thus, the behavior of the intra-cortical capillary network L1 does not differ from the behavior of a homogeneous random network when analyzed by box-counting or sandbox.

In addition, the power spectrum (Fig. A11(D)) also displays two domains: a saturated domain at low frequencies and a decreasing domain at high frequencies. In case of region L1, the cut-off frequency k_c between these two domains is 6.34 pixel^{-1}, corresponding to a cut-off length of $256/k_c$, *i.e.* 49.28 μm, which is very close to the values obtained by both sand-box methods. Above k_c, the power spectrum is linear, of slope = -4.79, very close to the slopes obtained by Risser et al. (2007) for healthy networks (-4.8 or -4.9). The linear range as detected by Berntson's procedure spans over half a decade of frequency scales (from 6.34 to 29.4 pixel^{-1}). Thus, when studied by the spectral approach, the behavior of the intra-cortical capillary network *L1* does not differ from the behavior of 3D homogeneous random networks (see Fig. A10), whose slope at high frequencies (-4.56) is also of same order of magnitude.

Similar results (see Table A2) have been obtained with every dataset studied, except for the box-counting slope at high scale for the summit regions S1 and S2, which is significantly smaller than 3. In this case, the maximal box size attainable due to the limited depth of the datasets once again precludes a homogeneous, space-filling behavior to be reached. However, the results obtained by the other methods (pseudo 3D sand-box and spectral methods) suggest that these summit regions are effectively space-filling at large scale.

[8] As pointed out by an anonymous reviewer, because the images acquired by Risser et al. (2007) are so well resolved that the capillaries are much wider than the voxel size, this same phenomenon could also introduce some bias in their analysis. In this context, it is noteworthy that, when studied by box-counting, the behavior of homogeneous random 4-pixels thick meshes of characteristic length 40 pixels exhibits a linear domain (spanning from 2 to 16 as determined by Berntson's procedure) independent of the overlap of a resampled DLA tree. However, the slopes of these linear domains are different (-1.462 $\pm$ 5.6 10-4 (no overlap) and -1.692 $\pm$ 0.015 (overlap)), the difference being highly significant ($p<0.0001$ as tested by a single classification ANOVA with two groups). In addition, the last slope is very close to the fractal dimension of DLA in 2D (1.667).

All together, these results demonstrate that healthy intra-cortical capillary networks are space filling over a cut-off length of order 25 to 75 μm, which should give an estimate of the characteristic length of the capillary lattice. Indeed, these values are in close correspondence with the mean capillary length (57.37 to 63.26 μm) determined by Cassot et al. (2006). In addition, these values also are in accordance with the mean value of the extravascular distance (50 μm), which provides an alternative definition for the order of magnitude of the capillary mesh (Cassot et al. 2006).

However, even though it is tempting to conclude that healthy intra-cortical capillary networks are not fractal, but rather random, at lower scales, the analytical tools used above are inconclusive, because, once again, the obtained results are compatible with both behaviors. In other words, the analysis of the data does not permit to discriminate between true fractality and apparent (or artifactual) fractality. Therefore, additional investigations are needed to conclude on the nature of vascular networks at low scale. For that purpose, we introduce an alternative method based on the multi-scale analysis of the regional maxima of the distance map.. Indeed such an analysis keeps the essential information regarding the capillary mesh heterogeneities while avoiding artifacts due to the 3D nature of its elementary constituents (*i.e.* the capillaries).

(d) An alternative approach

In Risser et al. (2007), the box-counting and sand-box methods are used to analyze the vessels' network whereas the spectral approach is used to analyze its avascular space. Here, we propose a method allowing the study of the avascular space by the box-counting and sand-box methods. The idea is to provide a new tool for determining whether the volumes of tissue contained in each elementary capillary mesh span several orders of magnitudes or not.

i. Method

Briefly, the regional maxima of the distance map $d(i,j,k)$, *i.e.* the connected components of voxels with a constant d value and whose external boundary pixels all have a lower d value, are first computed (see Fig. 3 for a simultaneous representation of these regional maxima and of the vascular network in a sub-volume of region L1) and, after cropping by 4 voxels on lateral faces to remove side effects, are subsequently analyzed using the box-counting and both sand-box methods. This procedure has first been validated in 2D by using a fractal mesh-like structure containing empty spaces with surfaces spanning more than five orders of magnitude, the 8th order inverted Sierpinski carpet (Baish & Jain 2000). The set of the regional maxima of its distance map was studied by the box-counting and the sand-box methods. In both cases, a fractal behavior was demonstrated. The box-counting (respectively the sand-box) fractal dimension was 1.884 (respectively 1.845). The linear range determined by Berntson's procedure spanned from 1 to 4096 pixels, *i.e.* the whole range of scales under study (respectively from 3 to 1259 pixels, *i.e.* more than two decades). In both cases, the coefficient of determination R^2 was greater than 0.999.

ii. Analysis of intra-cortical capillary networks

The results obtained for region L1 are displayed on Fig. A12. First, regarding box-counting, the log-log plot of N versus r does not exhibit any linear domain, which is confirmed by use of Berntson's procedure. Instead, a continuous variation in its local slope is obtained and no clear cut-off scale can be identified. A similar behavior is obtained with the

sand-box method (dots in Fig. A12(B)). Second, regarding the pseudo 3D sand-box (continuous line in Fig. A12(B)), a linear domain, of slope 1.981, is detected by Berntson procedure for r between 47.58 and 152.5 µm. Below, a continuous variation in the local slope is observed.

Regarding the box-counting method, similar results have been obtained for every dataset studied. Regarding sand-box methods, similar results have also been obtained except that, in addition, a linear domain at very low scale (typically half a decade, between 5 and 25 µm) has been evidenced in several regions. In regions L3 and LA1, such a domain has been found by both sand-box methods, whereas in regions L2 and S1 such a domain has been found by only one of them. However, even in these cases, no clear cut-off scale could be deduced.

These results clearly demonstrate that the distributions of regional maxima of healthy capillary networks are not fractal at low scale. Thus, at low scale, healthy capillary networks are homogeneous. The fractal behavior of the capillaries of a middle layer cortical region deduced by Cassot et al. (2006) using the box-counting method was therefore purely artifactual. Of course, this comment doesn't hold for the fractal behavior of the intra-cortical tree-like vascular structures evidenced by the same authors after having separated these structures from the capillary lattice.

APPENDIX B: Resolution of the pressure field of Poiseuille flow using fictitious random walkers

The steady flow of fluid through a pipe of circular cross section is a well known exact analytical solution of the Navier-Stokes equations, displaying a parabolic velocity profile and a linear pressure drop. In this type of flow, diffusion is negligible compared to convection. As a consequence, fluid particles (i.e. infinitesimal volumes of fluid large enough to contain many molecules) do not physically behave as random walkers but rather deterministically follow straight trajectories. Nevertheless, the pressure field of Poiseuille flow, which, according to the Navier-Stokes equations is governed by:

$$\frac{\partial^2 p}{\partial x^2} = 0 ,$$

where x is the longitudinal coordinate, can be solved using fictitious random walkers, as illustrated below, from the known entry and outlet pressures (p_{in} and p_{out}).

First, this differential equation is approximated on a square grid (i,j) by a finite difference method, leading to:

$$p_{i,j} = \frac{1}{2}\left(p_{i-1,j} + p_{i+1,j}\right).$$

This recursive equation can be interpreted as a set of transition probabilities that determine the motion of fictitious random particles according to the following rules: if a particle is at position (i,j) at step K, then, at step K+1, the particle goes to (i-1,j) with probability 0.5 or to (i+1,j) with probability 0.5 (Zwillinger 1998).

For each position (i,j) of the grid, the value of the pressure $p_{i,j}$ is approximated by launching a large number N of particles from (i,j). When a particle n reaches the inlet or outlet boundaries, the particle is stopped and the pressure value on the boundary is stored ($p^n = p_{in}$ or p_{out}). An approximation to the solution, at the point (i,j), is given by the average $\frac{1}{N}\sum_{n=1}^{N} p^n$ of all the values stored. Of course, the numerical accuracy of this approach increases with increasing N, as displayed on Figs. B1 and B2.

As a conclusion, the use of random walkers as a tool do not need to be supported by a physical reality, where real random walkers are moving, in order to describe physical processes. In the case of a Poiseuille flow, the relevant physics is purely convective : diffusion is negligible and, as a consequence, fluid particles do not follow random walks but determinist straight trajectories. However, statistics performed over the trajectories of a large number of fictitious random walkers allow to evaluate the pressure field, which is a physical reality.

APPENDIX C. Justification for using a DLA growth process for modeling vascular morphogenesis

The justification for using a DLA growth process, well known to produce highly branched fractals structures, during the steps 2 and 4 of Fleury's model, as described in Section 3, is based on the analogy between DLA and Dielectric Breakdown (DB) (Niemeyer et al. 1984, Vicsek 1992), which is itself formally identical to the selection of capillary vessels by shear stress in a laplacian pressure field to remodel into arteries or veins (Fleury & Schwartz 1999).

Indeed, a capillary lattice may be considered as a porous media. If, as a crude approximation, its permeability k is assumed to be isotropic and uniform, implying that each capillary has the same radius R, and if the blood is assumed to be incompressible and newtonian, the flow $\boldsymbol{q}$ is governed by Darcy's law:

$$\boldsymbol{q} = -(k/\mu).\mathbf{grad}(P),$$

where μ is the dynamic viscosity and P is the pressure. If the medium if further assumed to be non-deforming, the continuity equation leads to a laplacian pressure field (Bear 1972):

$$\Delta P = 0.$$

In addition, under the same hypotheses, the flow in each capillary tube must be a Poiseuille's flow, with a parabolic velocity profile. Thus, in each capillary tube, the wall shear stress τ can be evaluated as $4\mu V/R$, where V is the mean tube velocity. The pressure gradient can be related to the local flow ($\pi R^2 V$) by Poiseuilles's law:

$$\mathrm{grad}(P) = -8\mu(\pi R^2 V)/(\pi R^4) = -8\mu V/R^2.$$

Thus, in each capillary tube, the wall shear stress can be related to the pressure gradient by:

$$\tau = -R.\mathrm{grad}(P)/2.$$

If the probability p for a given capillary to enlarge, becoming an arterial segment under the action of flow, is proportional to the wall shear stress, then:

$$p = -K\,\mathrm{grad}(P),$$

where K is proportional to the time scale of the sequence from membrane transduction to cellular reactions, in interaction with perivascular cells and matrix components, until a large vessel has been completed (Fleury 1999). Finally, if the pressure drop in arterial segments is neglected (*i.e.* if the hydraulic resistance of the arterial segments is supposed to be negligible compared to the resistance of the capillaries), then, the pressure along the arterial arborescence is constant and imposed by the pressure at the arterial entry points.

This problem is formally identical to DB, introduced in order to simulate phenomena ranging from atmospheric lightning to electric treeing in polymers. In these cases, if a sufficient voltage difference is imposed, a conducting phase invades an insulating material, exhibiting a randomly branched, fractal structure. The growth velocity of this conducting phase is stochastically proportional to the local electric field ($\boldsymbol{E} = -\,\mathbf{grad}\,\phi$), whereas the electric potential ϕ satisfy Laplace's equation ($\Delta\phi = 0$). The conducting phase is assumed to be equipotential (infinitely conducing). Thus, in DB, the growth probability depends on the local field (potential) determined by the equipotential growing pattern.

Finally, it is well known that DB is equivalent to DLA, except for a slight difference in the boundary conditions (Vicsek 1992): the sticking condition used in DLA corresponds to an equipotential in the sites adjacent to the growing aggregate whereas, in DB, the equipotential is the growing pattern itself. As a consequence, a DLA growth process is well suited to model the growth of the arterial and venous trees in steps 2 and 4 of Fleury's model.

Acknowledgements: F. Lauwers (INSERM U855) must be thanked for his skillful guiding through the intra-cortical vascular labyrinth. We wish to thank V. Fleury (CNRS UMR7057) for inspiring discussions, P. Duru (CNRS UMR5502), AJM. Cornelissen (CNRS UMR7057) and L. Pitchford (CNRS UMR5213) for carefully reading the manuscript and suggesting constructive improvements. We are grateful to M. Quintard and J. Magnaudet (CNRS UMR5502) for continuous support. This work has been partly supported by ACI Technologies pour la Santé, Grant No. 02 TS 031, of the French Department of Education, Research and Technology and by the CNRS (PEPS ST2I 2008).

References :

Al-Kilani, A., Lorthois, S.,. Nguyen, T.H, le Noble, F., Cornelissen, A., Unbekandt, M., Boryskina, O., Leroy, L. & Fleury, V. 2008 During vertebrate development, arteries exert a morphological control over the venous pattern through physical factors. *Phys. Rev. E*, **77**, 051912-1 - 051912-16 .

Arlt, C., Schmid-Schönbein, H. & Baumann, M. 2003 Measuring the fractal dimension of the microvascular network of the chorioallantoic membrane. *Fractals* **11**, 205 - 212.

Baish, J.W. & Jain, R.K. 2001 Reply to Chung, H.W. & Chung H.J. Correspondence re: J. W. Baish and R. K. Jain, Fractals and Cancer. *Cancer Res.* **61**, 8348 - 8350.

Baish, J.W. & Jain., R.K. 2000 Fractals and cancer. *Cancer Res.* **60**, 3683 - 3688.

Bear, J. 1972 *Dynamics of fluids in porous media.* New York: American Elsevier Publishing Company.

Bergman, D.L. & Ullberg, U. 1998 Scaling properties of the placenta's arterial tree. *J. Theor. Biol.* **193**, 731 - 738.

Berntson, G.M. & Stoll, P. 1997 Correcting for finite spatial scales of self-similarity when calculating the fractal dimensions of real-world structures. *Proc. Roy. Soc. Lon. B*, **264**, 1531 - 1537.

Cassot, F., Lauwers, F., Fouard, C., Prohaska, S. & Lauwers-Cances, V. 2006 A novel three-dimensional computer-assisted method for a quantitative study of microvascular networks of the human cerebral cortex. *Microcirculation* **13**, 1 - 18.

Codling, E.A., Plank, M.J. & Benhamou, S. 2008 Random walk models in biology. *J. R. Soc. Interface* **5**: 813-834.

Courant, R., Friedrichs, L. & Lewy, H. 1928 Über die Partiallen Differenchengleichungen der Mathematischen Physik. *Mathematische Annalen***100**, 32-74.

Duvernoy, H.M., Delon, S. & Vannson, J.L. 1981 Cortical blood vessels of the human brain. *Brain Res Bull.* **7**: 519-579.

Fleury, V. & Schwartz, L. 1999 Diffusion limited aggregation from shear stress as a simple model of vasculogenesis. *Fractals* **7**, 33 - 39.

Fleury, V. & Schwartz, L. 2000 Modelisation of 3-D microvasculature by interlaced diffusion limited aggregation. *Fractals* **8**, 255 - 259.

Fleury, V. & Schwartz, L. 2001 A link between dendritic growth and remodeling of blood vessels. In *Branching in nature* (eds. V. Fleury *et al.*), pp. 293 – 303. Les Ulis: EDP Sciences.

Fleury, V. 2000 Branching morphogenesis in a reaction-diffusion model. *Phys. Rev. E.*, **61**, 4156 - 4160.

Gan, R.Z., Tian, Y., Yen, R. T. & Kassab, G. S. 1993 Morphometry of the dog pulmonary venous tree. *J. Appl. Physiol.* **75**, 432 - 440.

Gaudio, E., Chaberek, S., Montella, A., Pannarale, L., Morini, S., Novelli, G., Borghese, F., Conte, D. & Ostrowski, K. 2005 Fractal and Fourier analysis of the hepatic sinusoidal network in normal and cirrhotic rat liver. *J. Anat.* **207**, 107 -115.

Gazit, Y., Berk, D.A., Leunig, M., Baxter, L.T. & Jain, R.K. 1995 Scale-invariant behavior and vascular network formation in normal and tumor tissue. *Phys. Rev. Lett.* **75**, 2428 - 2431.

Georgiadis, J.G., Noble, D.R. and Buckius, R.O. 1996 Questions in fluid mechanics – Tortuous micro-flow in large disordered packed beds. *J. Fluid Eng. Trans. ASME.* **118**, 434 – 436.

Gödde, R. & Kurz, H. 2001 Structural and biophysical simulation of angiogenesis and vascular remodeling. *Dev. Dyn.* **220**, 387 - 401.

Grizzi, F., Colombo, P., Barbieri, B., Franceschini, B., Roncalli, M.& Chiriva-Internati, M. 2001 Correspondence re: E. Sabo et al., Microscopic Analysis and Significance of Vascular Architectural Complexity in Renal Cell Carcinoma. *Clin. Cancer Res.* **7**, 3305 - 3306.

Hahn, H.K., Evertsz, C.J.G., Fasel, J.H.D. & Peitgen, H.O. 2003 Fractal properties, segment anatomy, and interdependence of the human portal vein and the hepatic vein in 3d. *Fractals* **11**, 53 - 62.

Halley, J.M., Hartley, S., Kallimanis, A.S., Kunin, W.E., Lennon, J.J. & Sgardelis, P. 2004 Uses and abuses of fractal methodology in ecology. *Ecology Letters* **7**, 254 - 271.

Hamburger, D., Biham, O. & Avnir, D. 1996 Apparent fractality emerging from models of random distributions. *Phys. Rev. E* **53**, 3342 - 3358.

Heinzer, S., Krucker, T., Stampanoni, M., Abela, R., Meyer, E.P., Schuler, A., Schneider, P. & Müller, R. 2006 Hierarchical microimaging for multiscale analysis of large vascular networks. *Neuroimage* **32**, 626-636.

Herman, P., Kocsis, L. & Eke, A. 2001 Fractal branching pattern in the pial vasculature in the cat. *J. Cereb. Blood Flow Metab.* **21**, 741 - 753.

Honda, H. & Yoshizato, K. 1997 Formation of the branching pattern of blood vessels in the wall of the avian yolk sac studied by a computer simulation. *Develop. Growth. Differ.* **39**, 581 - 589.

Jain, R.K. 1988 Determinants of tumor blood flow: a review. *Cancer Res.,* **48**, 2641 - 2658.

Jiang, Z.L., Kassab, G. S. & Fung, Y. C. 1994 Diameter-defined Strahler system and connectivity matrix of the pulmonary arterial tree.. *J. Appl. Physiol.* **76**, 882 – 892.

Kassab, G.S. 2000 The coronary vasculature and its reconstruction. *Ann. Biomed. Eng.* **28**, 903 - 915.

Kirchner, L.M., Schmidt, S.P., & Gruber, B.S. 1996 Quantitation of angiogenesis in the chick chorioallantoic membrane model using fractal analysis. *Microvasc. Res.* **51**, 2 - 14.

Lauwers, F., Cassot, F., Lauwers-Cances, V., Puwanarajah, P. & Duvernoy, H. 2008 Morphometry of the human cerebral cortex microcirculation: general characteristics and space-related profiles. *Neuroimage*, **39**, 936 - 948.

le Noble, F.A., Moyon, D., Pardanaud, L., Yuan, L., Djonov, V., Matthijsen, R., Bréant, C., Fleury, V. & Eichmann, A. 2004 Flow regulates arterial-venous differentiation in the chick embryo yolk sac. *Development* **131**, 361 - 373.

Mantzaris, N.V., Webb, S. & Othmer, H.G. 2004 Mathematical modeling of tumor-induced angiogenesis. *J. Math. Biol.* **49**, 111 - 187.

Masters, B.R. 2004 Fractal analysis of the vascular tree in the human retina. *Annu. Rev. Biomed. Eng.* **6**, 427 - 452.

Meakin, P., Sun, T. & Jøssang, T. 2001 Branched patterns in geology: Rivers and other systems. In *Branching in nature* (eds. V. Fleury *et al.*), pp. 119 – 159. Les Ulis: EDP Sciences.

Merks, R.M.H., Perryn, E.D., Shirinifard, A. and Glazier, J.A. 2008 Contact-inhibited chemotaxis in De Novo and sprouting blood-vessel growth. *PLOS Comp. Biol.* **4**, e1000163.

Murray, J.D. 1995 Use and abuse of fractal theory in neuroscience. *J. Comp. Neurol.* **361**, 369 - 371.

Nguyen, T.H., Eichmann, A., le Noble, F. & Fleury, V. 2006 Dynamics of vascular branching morphogenesis: The effect of blood and tissue flow. *Phys. Rev. E* **73**, 061907-1 - 061907-14.

Niemeyer, L., Pietronero, L. & Wiesmann, H.J. 1984 Fractal Dimension of Dielectric Breakdown. *Phys. Rev. Lett.* **52**, 1033 - 1036.

Panico, J. & Sterling P. 1995 Retinal neurons and vessels are not fractal but space-filling. *J. Comp. Neurol.* **361**, 479 - 490.

Parsons-Wingerter, P., Lwai, B., Yang, M.C., Elliott, K.E., Milaninia, A., Redlitz, A., Clark, J.I. & Helene Sage, E. 1998 A novel assay of angiogenesis in the quail chorioallantoic membrane: stimulation by bfgf and inhibition by angiostatin according to fractal dimension and grid intersection. *Microvasc. Res.* **55**, 201 - 214.

Patan, S. 2000 Vasculogenesis and angiogenesis as mechanisms of vascular network formation, growth and remodeling. *J. Neuro-Oncology* **50**, 1 - 15.

Plank, M.J. & Sleeman, B.D. 2004 Lattice and non-lattice models of tumor angiogenesis. *Bull. Math. Biol.* **66**, 1785 - 1819.

Pries , A.R., Secomb., T.W., Gaehtgens, P. and Gross, J.F. 1990 Blood flow in microvascular networks. Experiments and simulation. *Circ. Res.* **67**, 826 – 834.

Risau, W. 1997 Mechanisms of angiogenesis. *Nature* **386**, 671 - 674.

Risser, L. 2007 Analyse quantitative de réseaux micro-vasculaires intra-corticaux. Ph.D. Thesis, Université Paul Sabatier, Toulouse, France.

Risser, L., Plouraboué, F., Steyer, A., Cloetens, P., Le Duc, G. & Fonta, C. 2007 From homogeneous to fractal normal and tumorous microvascular networks in the brain. *J. Cereb. Blood Flow Metab.* **27**, 293 - 303.

Russ, J.C. 1994 *Fractal surfaces*, pp. 191 – 224. NewYork: Plenum Press.

Sabo, E. & Resnick, M.B. 2001 Reply *Clin. Cancer Res.* **7**, 3307 - 3307.

Sabo, E., Boltenko, A., Sova, Y., Stein, A., Kleinhaus, S. & Resnick, M.B. 2001 Microscopic analysis and significance of vascular architectural complexity in renal cell carcinoma. *Clin. Cancer Res.* **7**, 533 - 537.

Sandau, K. & Kurz, H. 1997 Measuring fractal dimension and complexity — an alternative approach with an application. *J. Microscopy* **186**, 164 - 176.

Sokal, R.R. & Rohlf, F.J. 1994 *Biometry, Third edition.* San Francisco: W.H. Freeman.

Tosin, A., Ambrosi, D., & Preziosi, L. 2006 Mechanics and chemotaxis in the morphogenesis of vascular networks. *Bull. Math. Biol.* **68**, 1819 - 1836.

Turcotte, D.L., Pelletier, J.D. & Newman, W.I. 1998 Networks with side branching in biology. *J. Theor. Biol.* **193**, 577 - 592.

Vico, P.G., Kyriacos, S., Heymans, O., Louryan S. & Cartilier, L. 1998 Dynamic study of the extraembryonic vascular network of the chick embryo by fractal analysis. *J. Theor. Biol.* **195**, 525 - 532.

Vicsek, T. 1992 *Fractal Growth Phenomena* Singapore: World Scientific.

West, G.B., Brown, J.H. & Enquist, B.J. 1999 The fourth dimension of life: fractal geometry and allometric scaling of organisms. *Science* **284**, 1677 - 1679.

Weyn, B., Tjalma, W.A.A., Vermeylen, P., Van Daele, A., Van Marck, E. & Jacob, W. 2004 Determination of tumour prognosis based on angiogenesis-related vascular patterns measured by fractal and syntactic structure analysis. *Clin. Oncol.* **16**, 307 - 316.

Wilting, J., Birkenhäger, R., Eichmann, A., Kurz, H., Martiny-Baron, G., Marmé, D., McCarthy, J.E.G., Christ, B. & Weich, H.A. 1996 VEGF121Induces Proliferation of Vascular Endothelial Cells and Expression offlk-1without Affecting Lymphatic Vessels of the Chorioallantoic Membrane. *Dev. Biol.* **176**, 76 - 85.

Witten, T.A. & Sander, L.M., 1983 Diffusion-limited aggregation. *Phys. Rev. B* **27**, 5686 - 5697.

Yao, X., Qian, C-N., Zhang, Z-F.,. Tan, M-H, Kort, E., Yang, X.J., Resau, J.H. & Teh, B.T. 2007 Two distinct types of blood vessels in clear cell renal cell carcinoma have contrasting prognostic implications. *Clin. Cancer Res.* **13**, 161 - 169.

Zwillinger, D. 1998 *Handbook of differential equations (3rd edition)* San Diego : Academic press.

TABLES: All tables appear above the corresponding table legend

	Network type	*Resolution (µm/pixel)*	*Image size (pixels)*	*Image size (mm^2)*	*Image processing*	*Box cut-offs (µm)*	*2D box-counting fractal dimension*	*Refs*
Low resolution	Subcutaneous AV	~ 20	280 x 280	~ 5.6 x 5.6	S (n=12)	NA	1.70 ± 0.03	Gaz95, Bai01
	Developing CAM (ID 15)	11	512 x 512	5.6 x 5.6	E (n=23)	NA	1.416 ± 0.046 - 1.485 ± 0.037	San96
	Developing CAM (ID 13 – ID 18)	NA, NC	NA	NA	S (n=3 - 32)	100 - 7900	~ 1.1 – 1.8	Kir96
	Developing CAM (ID 13)	11	NA	NA	B (n=6)	22 - 220	1.26 ± 0.03	Wil96
	Developing CAM (ID 3 – ID 6)	~ 80	640 x 480	~ 5 x 3.5	S	~ 160 - NA	1.3 - 1.68	Vic98
	Developing CAM (ID 6 – ID 12)	5, NC	480 x 480	2.4 x 2.4	B	5 - 2400	~ 1.6 – 1.75	Par98
					S		1.37 ± 0.01 - 1.54 ± 0.03	
	Placenta's arterial*	85	2300 x 2900	195 x 220	E (n=22)	1700 - 17000	1.86	Ber98
	Pial vasculature	12.5	640 x 480	8 x 6	S (n=6)	NA	1.31 ± 0.03	Her01
	Retinal vasculature	NA, NC	NA	NA	S (n=10)	NA	1.7 ± 0.02	Mas04
High resolution	Subcutaneous capillary	~ 2	280 x 280	~ 0.56 x 0.56	S (n=12)	NA	1.99 ± 0.01	Gaz95, Bai01
	Epifoveal vessels	NA, CR	NA	~ 0.9 x 0.9	B (n=1)	NA	2.00	Pan95
	Developing CAM (ID 14)	0.98	1110 x 766	1.1 x 0.75	B (n=4)	NA	1.86 ± 0.01	Arl02
	Hepatic sinusoidal network (superficial layer)	SEM	NA	NA	E (n=39)	NA	2.01 ± 0.01	Gau05

Table 1: Synthetic summary of the 2D box-counting fractal dimensions in various types of healthy vascular network, at different scales of observation. Image processing: B (Box-counting), E (Box counting after edge detection), S (Box counting after skeletonizing), n (number of samples); Box cut-offs: values of the lower and upper cut-offs used for determining the fractal dimension by linear regression in a log-log plot (see Section 4).
Abbreviations used: AV: Arterio-Venous, CAM: Chorioallantoic membrane, ID: Incubation Day, SEM: Scanning Electron Microscopy; NA: not available; NC: No Capillaries: the experimental technique does not allow the observation of capillaries; CR: Capillaries Resolved: the experimental technique allows the observation of capillaries.
Symbols used: *: 3D organs: the box dimension has been estimated after projecting the vascular network in two dimensions; ~: estimates from the data available.

	Box-counting						
	Low scale			Cut-off	Large Scale		
	Slope	Linear range		r_{cut}	*Slope*	Linear range	
DLA + Grid	-1.318 ± 0.006	1 ± 0	10.4 ± 0.9	12.8 ± 1.8	-2 ± 0	16 ± 0	4096 ± 0
DLA + Random	-1.224 ± 0.003	2 ± 0	6 ± 0	10.8 ± 1.1	-1.999 ± 0.003	13.6 ± 2.2	4096 ± 0
	Sand-box						
	Low scale			Cut-off	Large Scale		
	Slope	Linear range		r_{cut}	*Slope*	Linear range	
DLA + Grid	1.727 ± 0.011	3 ± 0	28.6 ± 2.7	39 ± 0	1.973 ± 0.027	208 ± 98	2135 ± 840
DLA + Random	1.756 ± 0.014	3.4 ± 0.9	111 ± 20	152 ± 15	1.979 ± 0.008	230 ± 28	2511 ± 0

Table A1: Cut-off length, slopes and linear ranges obtained by Berntson's procedure for box-counting (upper panel) and sand-box (lower panel) performed over five realizations of 5000 particles resided DLA clusters superimposed to a square grid (DLA + Grid) or random networks (DLA + Random). In all cases, the slopes were determined with coefficients of determination greater than 0.999.

	Box-counting			Pseudo 3D Sand-box			Power Spectrum	
	Low scale	Cut-off (µm)	Large Scale	Low scale	Cut-off (µm)	Large Scale	Cut-off (µm)	Large Scale
	Slope	r_{cut}	*Slope*	*Slope*	r_{cut}	*Slope*	r_{cut}	*Slope*
L1	-2.179	26.3	-3	1.595	47.6	1.949	40.4	-4.787
L2	-2.241	26.3	-3	1.629	62.2	2.014	40.4	-4.656
L3	-2.251	26.3	-3	1.624	47.6	1.924	48.0	-4.31
LA1	-2.265	26.3	-2.977	1.700	62.2	1.957	48.0	-4.418
S1	-2.224	26.3	-2.5	1.573	76.9	1.958	48.0	-4.444
S2	-2.227	26.3	-2.524	1.580	62.2	1.983	48.0	-4.602

Table A2: Cut-off length and slopes of the best linear fits for box-counting, pseudo 3D sand-box and spectral approach performed over six intra-cortical vascular networks, described in section A2.(a). In all cases, the slopes were determined with coefficients of determination greater than 0.99.

FIGURES: All figures appear below the corresponding figure legend

Figure 1: 672 x 672 highlight of generic patterns constructed using a square grid (above) and a random network (below). The characteristic length of the capillary lattice, denoted by *n,* has been fixed to 16. By resampling, the smallest scale in the quasi-fractal DLA-type tree is also *n* (which is equivalent to use random walkers of size *n* x *n* to construct the DLA, see Appendix A, Section A1(a)).

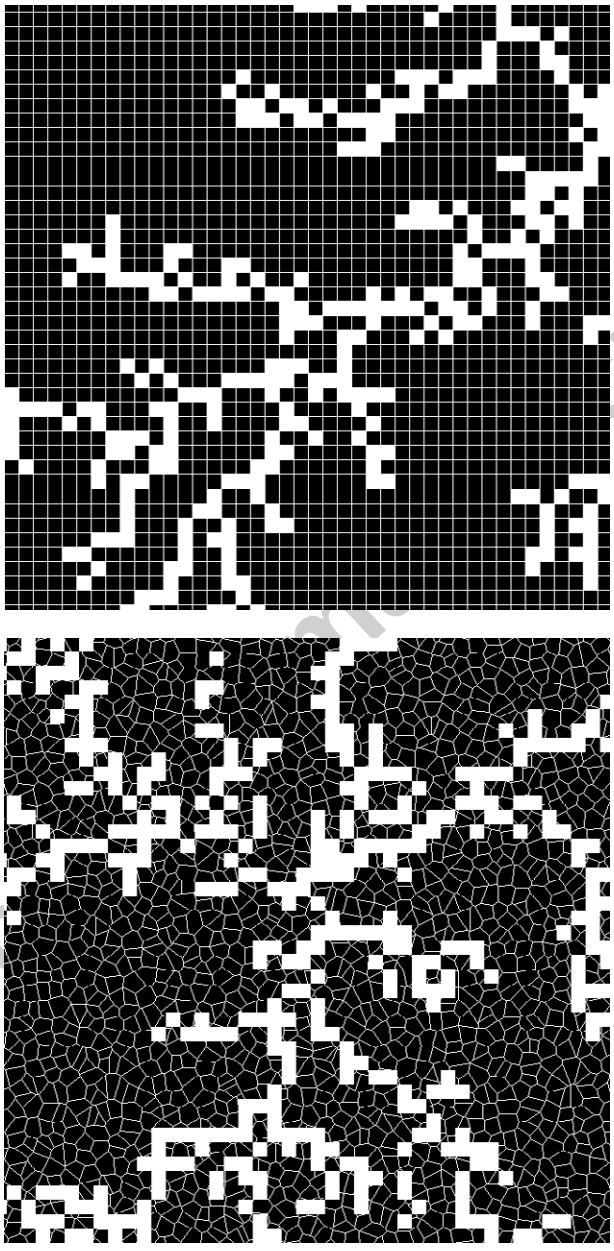

Figure 2: Volume rendering of a selection of representative datasets of healthy intra-cortical networks from the collateral sulcus in the temporal lobe (a) Capillary mesh in a lateral region of the sulcus (L1) ; (b) Capillary mesh surrounding the distal extremity of an arterial arborescence (indicated by stars) in a lateral region of the sulcus (LA1). The red box in Fig. 2(a) corresponds to a region highlighted in Fig. 3 ; (c) Capillary mesh in a top region of the sulcus (S1) ; (d) Capillary mesh in a top region of the sulcus, exhibiting a preferential orientation of vessels (S2).

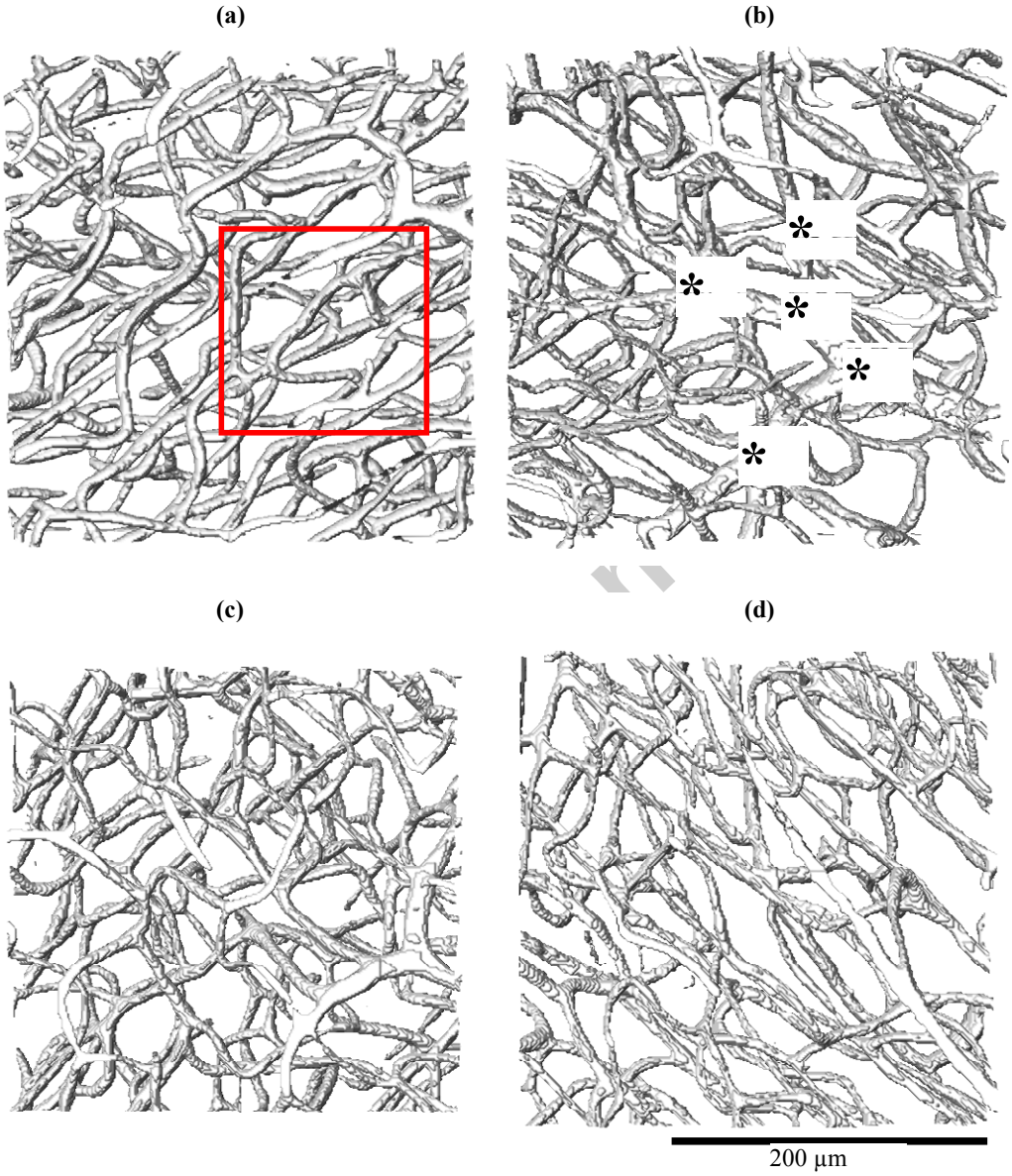

Figure 3: Simultaneous representation of the vascular network contained in the sub-volume of region L1 (~ 120 x 120 x 45 voxels) highlighted by the red box in Fig. 2a and of the regional maxima of the distance map of its avascular space. Two different views of the same area are provided. The colour-map is encoding for the depth (in voxels). The regional maxima of the avascular distance map are represented by dots.

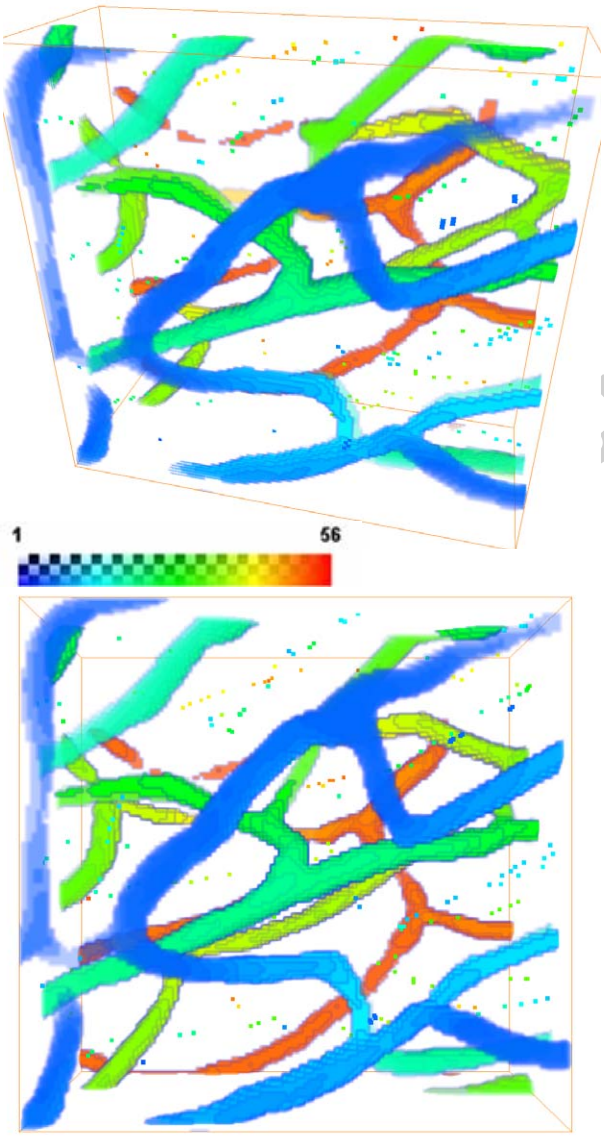

Figure A1: A random network exhibiting a Gaussian distribution of cells' areas. This network has been constructed by randomly choosing one point in every element of a 16 x 16 square grid in a 4096 x 4096 domain, and by subsequently extracting the voronoi diagram of this random set of points. A: Highlight of a 160 x 160 domain. Dotted lines: 16 x 16 square grid ; Dots: random set of points ; Lines: voronoi diagram. B: Histogram of cell's areas. Line: best fit of the data to a Gaussian function $f(x) = K\exp\left(\frac{-(x-\mu)^2}{2\sigma^2}\right)$.

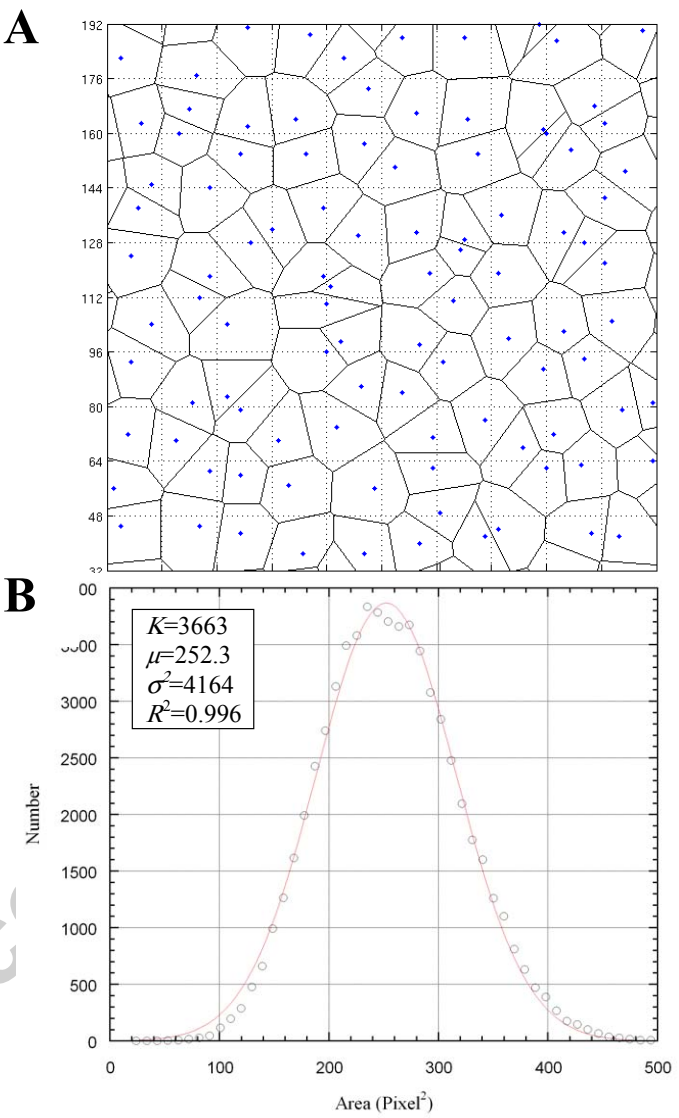

Figure A2: DLA cluster consisting of 500000 particles over a 4096 x 4096 domain.

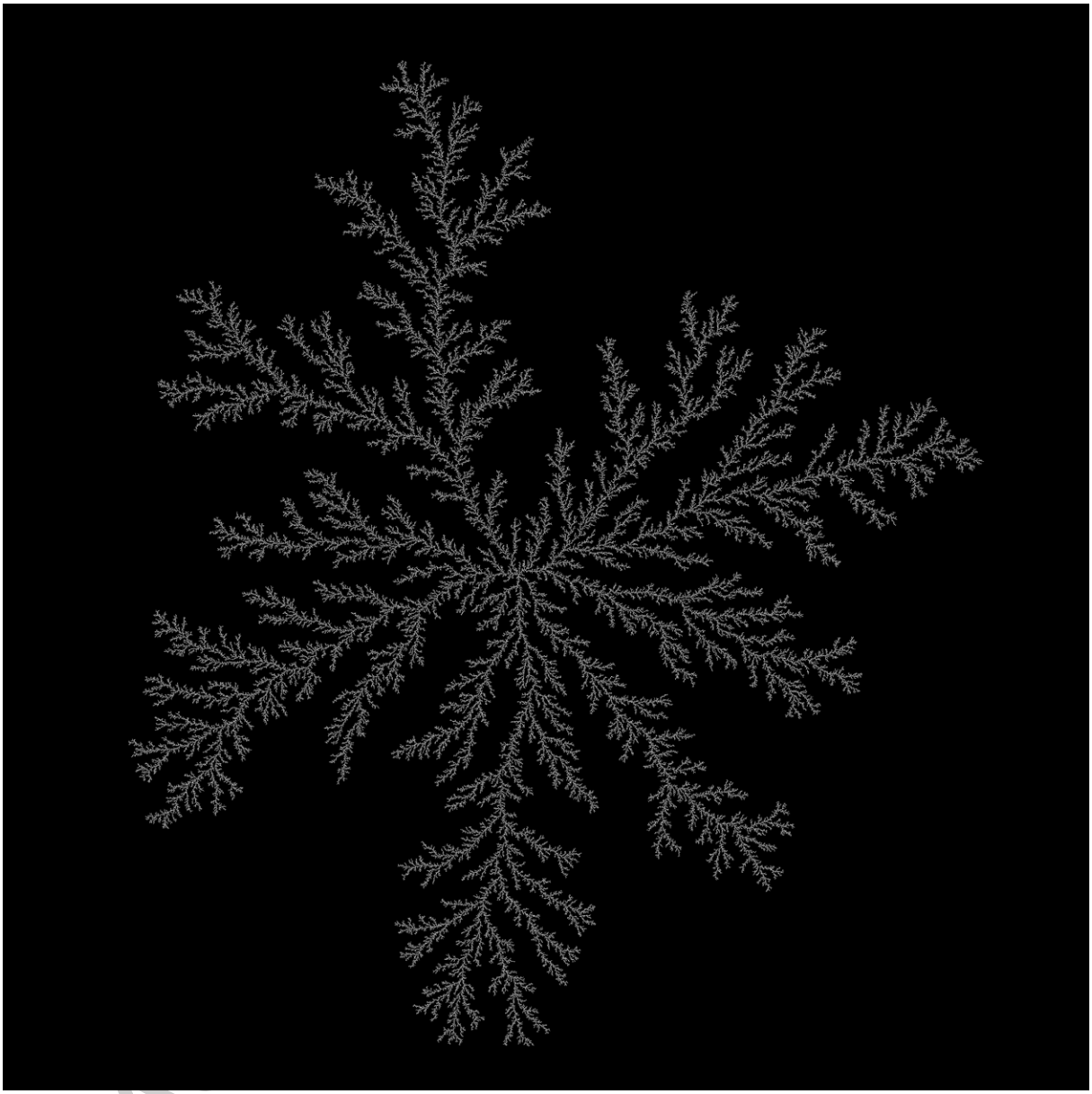

Figure A3: Box-counting analysis (A) and sandbox analysis (B) of the DLA cluster shown in Fig. A2: Continuous lines and symbols : N as a function of r. Dotted lines: best linear fit for box sizes included between r_{low} and r_{high}. This range represents the largest range for which a statistical test for curvilinearity is negative (see text).

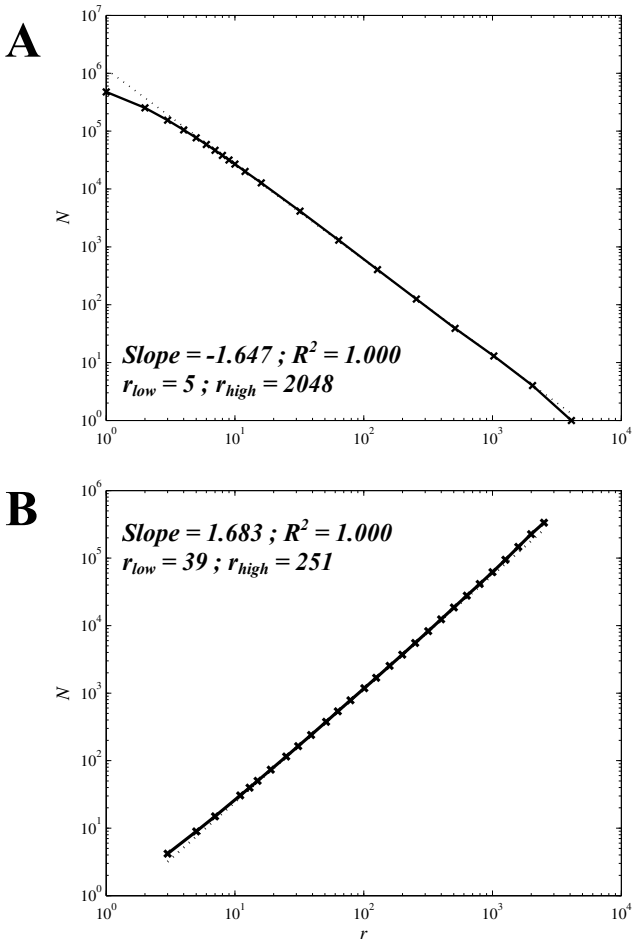

Figure A4: Box-counting analysis (A) and sand-box analysis (B) of a 5000 particles resampleed DLA cluster. Continuous lines and symbols: N as a function of r. Dotted lines: best linear fit for box sizes included between r_{low} and r_{high}. This range represents the largest range for which a statistical test for curvilinearity is negative (see text).

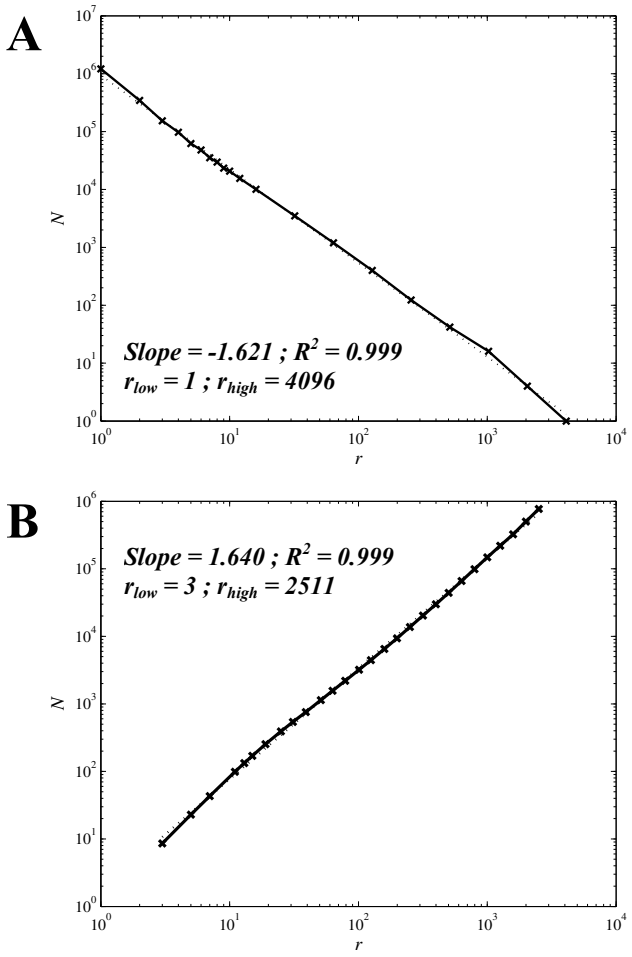

Figure A5: Box-counting analysis (A) and sand-box analysis (B) of a *n* x *n* square grid. Symbols: *N* as a function of *r*. Dotted lines: best linear fit for box sizes smaller than r_{cut}. Plain lines: best linear fit for box sizes larger than r_{cut}. For the ranges where a statistical test for curvilinearity is negative, see text.

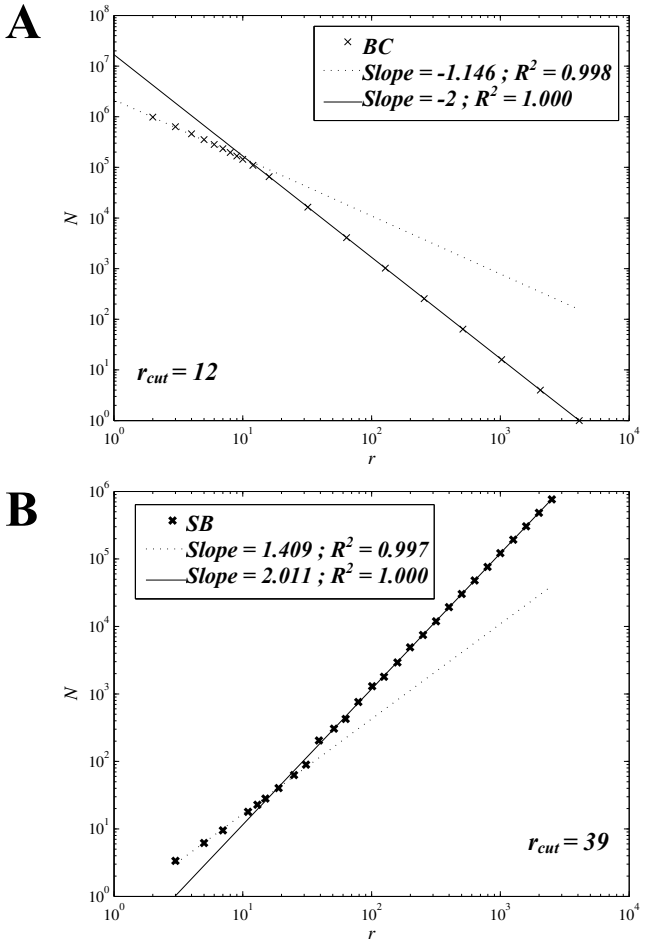

Figure A6: Box-counting analysis (A) and sand-box analysis (B) of a random network. Same conventions as in Fig. A5.

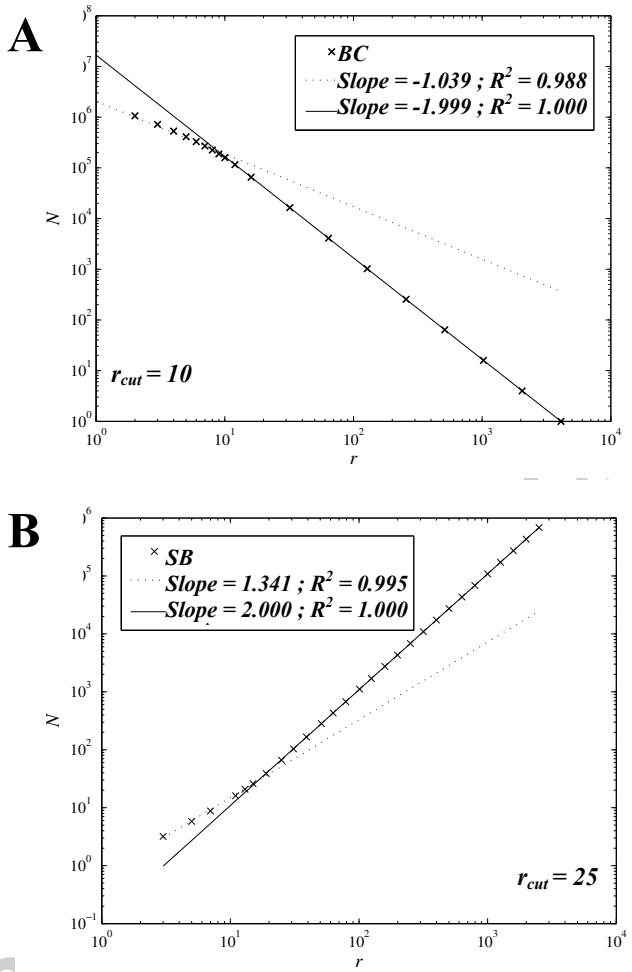

Figure A7: Box-counting analysis (A) and sand-box analysis (B) of a resampled DLA superimposed to a square grid. Same conventions as in Fig. A5. In addition, the points belonging to the linear range obtained by Berntson's procedure for $r < r_{cut}$ have been encircled by a dashed-dotted curve.

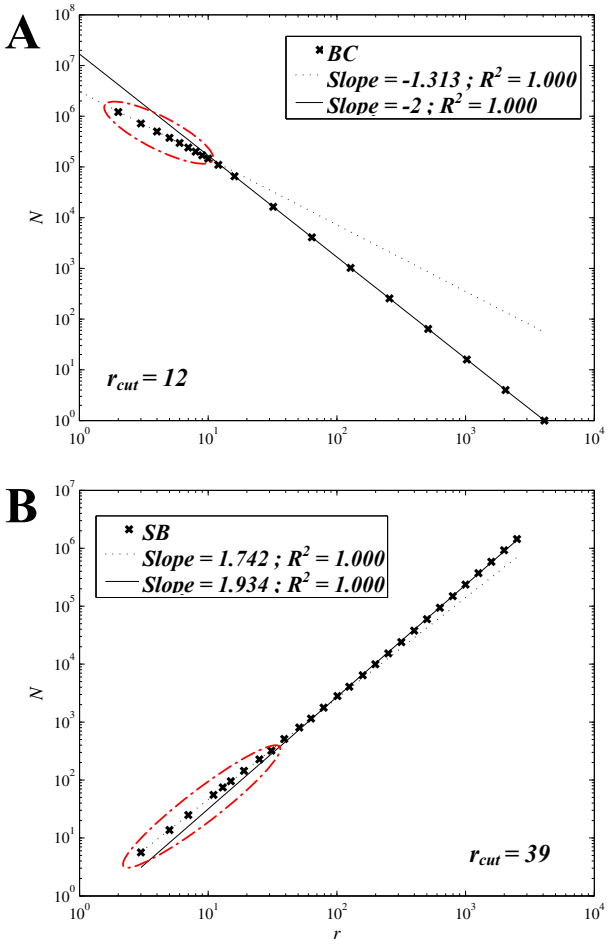

Figure A8: Box-counting analysis (A) and sand-box analysis (B) of a resampled DLA superimposed to a random network. Same conventions as in Fig. A5. In addition, the points belonging to the linear range obtained by Berntson's procedure for $r < r_{cut}$ have been encircled by a dashed-dotted curve.

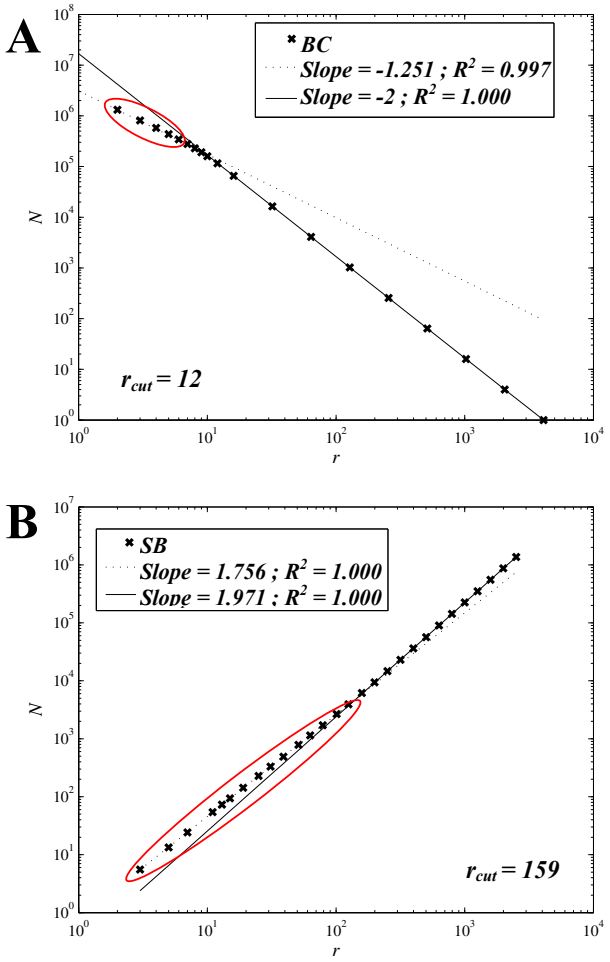

Figure A9: Power spectrum analysis of 5000 particles resampled DLA clusters superimposed, or not, to a square grid (A) or to random meshes (B). The averaged power spectrum P, averaged over five realizations, is displayed as a function of k_{ij}. Dots: DLA clusters ; Plain lines: Meshes ; Plain lines + Dots: DLA clusters superimposed to meshes ; Vertical dashed-dotted lines ; cut-off frequencies ; Dotted lines: Linear fits obtained using Berntson's procedure.

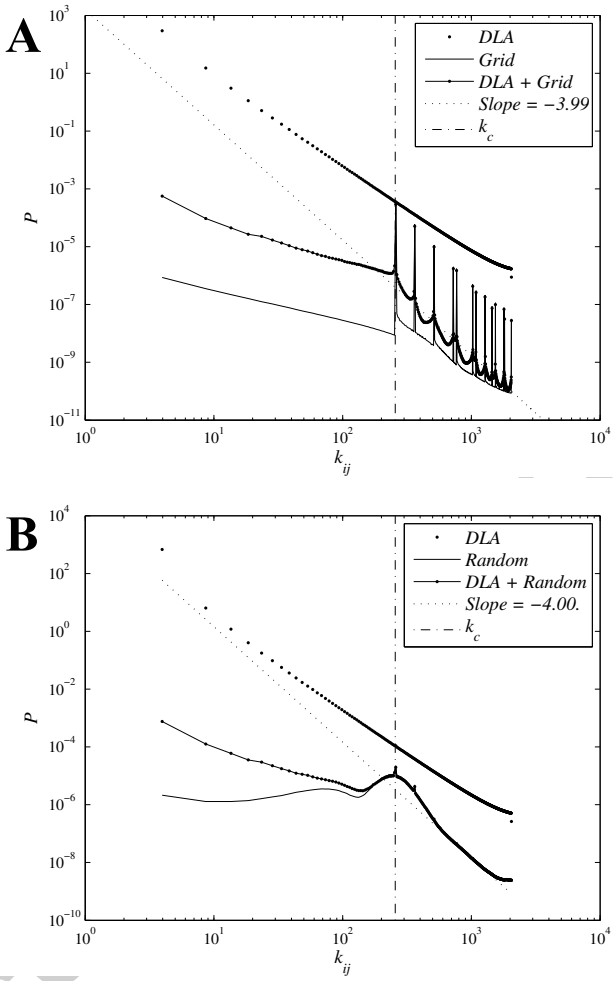

Figure A10: Power spectrum analysis of tri-dimensional random meshes. These meshes are constructed by generalizing the 2D procedure introduced in Section S1.(a): first, a random set of points is constructed by randomly choosing one point in every elements of a n x n x n cubic grid over a 256 x 256 x 64 domain ; second, the vertices of its voronoi diagram are extracted. The averaged power spectrum P, calculated as described in section S2, averaged over five realizations, is displayed as a function of k_{ij}. Vertical dashed-dotted line: cut-off frequency k_c = 15.5 (corresponding to a cut-off length of 256/ k_c = 15.5 pixels, very close to the size of the cubic grid used to generate the initial random set of points) ; Dotted line: Linear fit obtained using Berntson's procedure: the linear range spans from k_{ij} = 17.4 to 46.4, with a slope equal to -4.55 and a coefficient of determination greater than 0.998.

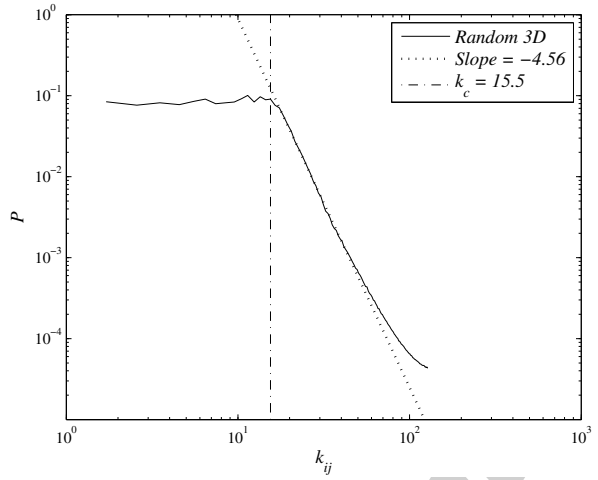

Figure A11: Box-counting (A), sand-box (B), pseudo 3D sand-box (C) and power-spectrum (D) analyses of the 256 x 256 x 64 voxel region of the healthy human intra-cortical vascular network L1 displayed in Fig. 2a: A, B and C: same conventions as in Fig. A5. In addition, the points belonging to the linear range obtained by Berntson's procedure for $r < r_{cut}$ have been encircled by a dashed-dotted curve ; D: same conventions as in Fig. A9.

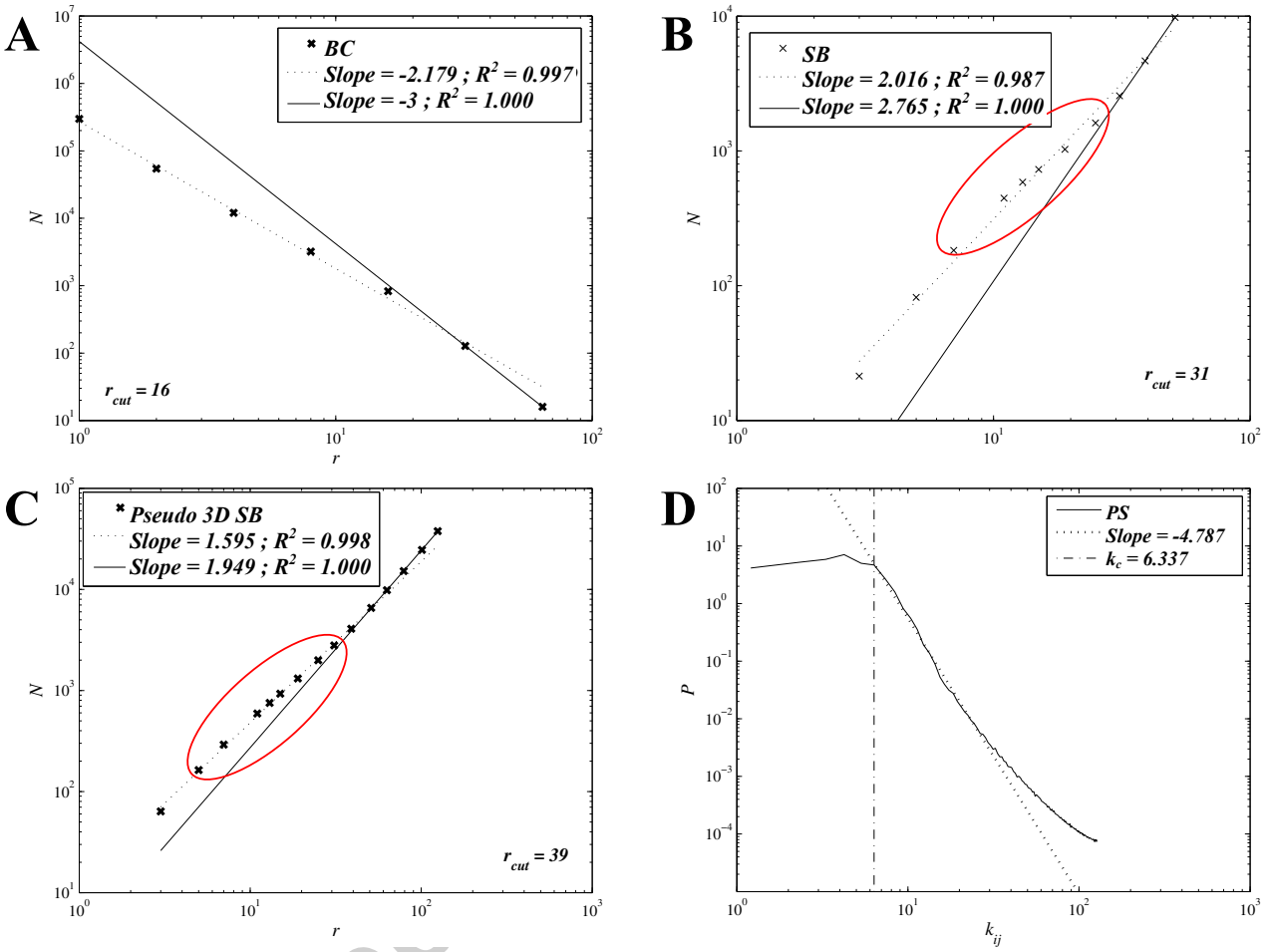

Figure A12: Box-counting (A) and sand-box (B) analyses of the regional maxima of the distance map of the healthy human intra-cortical vascular network L1. (A) Continuous line: N as a function of r ; (B) Continuous line: N as a function of r by pseudo 3D sand-box ; Dotted line: linear domain determined by Berntson's procedure ; Dots: N as a function of r by sand-box.

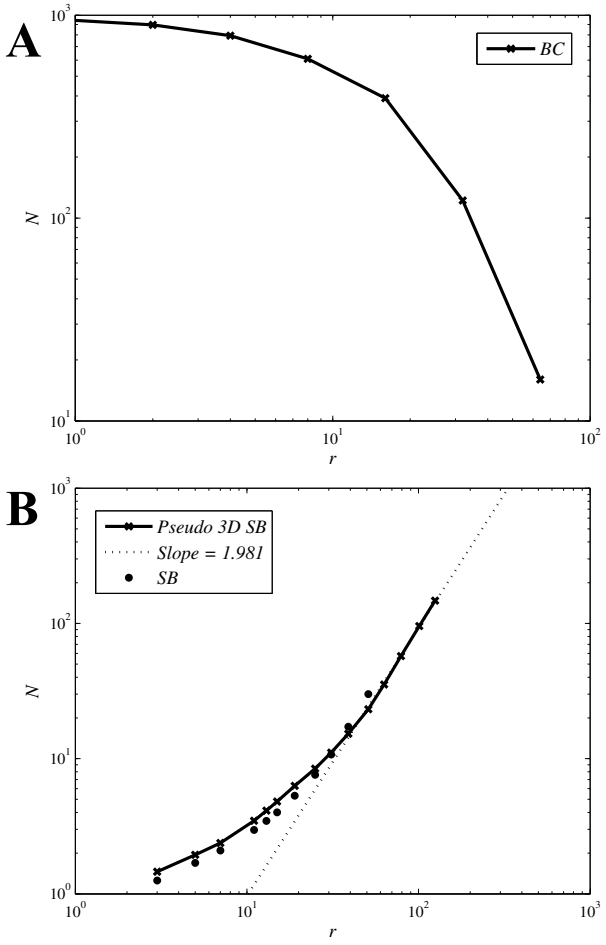

Figure B1: From top to bottom, iso-pressures obtained with $N = 10^3$, 10^4, 10^5 and 10^6. The exact solution of the Navier-Stokes equations predicts that iso-pressures are straight vertical lines. The "random walk" approach of resolution introduces noise, the intensity of which decreases when increasing the number of fictitious walkers.

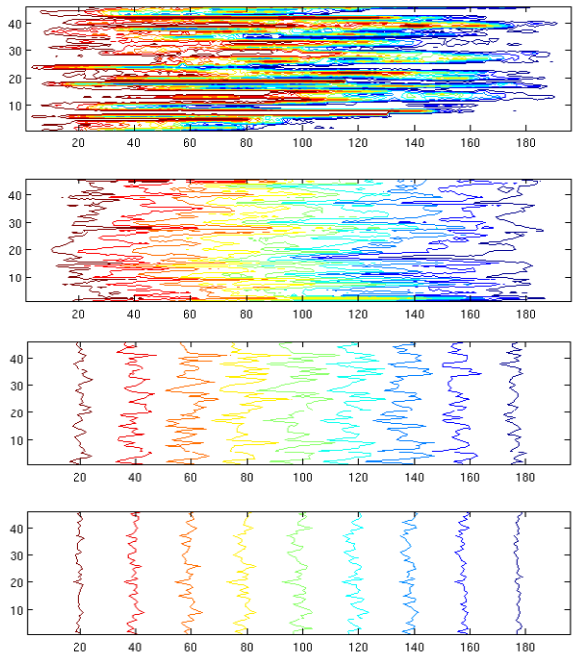

Figure B2: Mean pressure in each cross section. With N = 10^6, the well known linear decrease is obtained.